Pharmacological Research 178 (2022) 106156

Contents lists available at ScienceDirect

Pharmacological Research

journal homepage: www.elsevier.com/locate/yphrs

Review

Targeting BCR-Abl in the treatment of Philadelphia-chromosome positive chronic myelogenous leukemia

Robert Roskoski Jr.

Blue Ridge Institute for Medical Research, 3754 Brevard Road, Suite 106, Box 19 Horse Shoe, NC 28742-8814, United States

ARTICLE INFO

Keywords:
ATP-binding site
Protein kinase inhibitor classification
Protein kinase structure
Myristate-binding site
Regulation of Abl-1b enzyme activity
Specifically targeting the ABL myristoyl pocket

Chemical compounds studied in this article:
Asciminib (PubChem CID: 72165228)
Bosutinib (PubChem CID: 5328940)
Dasatinib (PubChem CID: 3062316)
5-(1
3-diaryl-1 H-pyrazol-4-yl)hydantoin
or DPH (PubChem CID: 660311)
GNF-2 (PubChem CID: 5311510)
GNF-5 (PubChem CID: 44129660)
Imatinib (PubChem CID: 5291)
Myristate (PubChem CID: 11005)
Nilotinib (PubChem CID: 644241)
Ponatinib (PubChem CID: 24826799)

ABSTRACT

Chronic myelogenous leukemia (CML) is an indolent malignant hematological disease that accounts for about 15% of all cases of leukemia. This disorder results from the formation of the Philadelphia chromosome that involves a reciprocal translocation that produces a lengthened chromosome 9 and shortened chromosome 22 – the Philadelphia chromosome. As a consequence of the translocation, the dysregulated BCR-Abl fusion oncoprotein is formed and it produces the abnormal proliferation of white blood cells. The treatment of CML with imatinib revolutionized the treatment of this disorder and led to the discovery and development of dozens of effective targeted protein kinase inhibitors. Imatinib (first generation), dasatinib, nilotinib, and bosutinib (second generation) have been FDA-approved for frontline therapy, and ponatinib (third generation) is approved for resistant disease with a *T315I* mutation. Each of these drugs is orally bioavailable. The BCR-Abl fusion protein lacks the physiological N-terminal myristoyl group that binds to a hydrophobic pocket in the large protein kinase lobe and inhibits enzyme activity. The absence of the myristoyl group leads to enhanced protein kinase catalytic activity. Asciminib was designed to bind to this binding pocket to reduce Abl kinase activity. Asciminib is orally effective and was FDA-approved as a third-line treatment for CML and a first-line treatment in patients with the *T315I* mutation. It blocks the activity of BCR-Abl by interacting with the myristate-binding site located 23 Å from the ATP-binding site and is the prototype of a type IV inhibitor. Asciminib is a so-called STAMP inhibitor that Specifically Targets the Abl Myristoyl Pocket.

1. Chronic myelogenous leukemia

Chronic myelogenous leukemia is an indolent, or slow-growing, malignant hematological disease characterized by leukocytosis (an elevated white blood cell count) [1,2]. There are generally an increased number of granulocytes (polymorphonuclear leukocytes), especially neutrophils. Peripheral blood smears may also reveal many immature cells or myeloblasts. Complete blood counts often exhibit low numbers of red blood cells, blood platelets, or both. Even though these findings may suggest leukemia, this diagnosis usually needs to be confirmed by other tests including those of the bone marrow. Signs and symptoms of CML may include fever, bone pain, unexplained weight loss, fatigue, and a sensation of left upper quadrant abdominal fullness (related to splenomegaly). However, about 20–50% of patients are asymptomatic at the time of presentation, and the diagnosis is based upon an abnormal blood count obtained during a routine medical examination. The median age at the time of the diagnosis is 67 years.

Chronic myelogenous leukemia accounts for about 15% of all cases of leukemia. The expected incidence of new cases in the United States in 2022 is 8860 (5120 males and 3740 females) and the expected number of fatalities is 1220 (670 males and 550 females). This compares with the incidence of lung cancers in 2022 at 237,000 (118,000 males and 119,000 females) and deaths at 130,000 (69,000 males and 61,000 females) [3]. The natural history of CML, prior to the advent of small molecule protein kinase antagonists, is progression from a stable or chronic phase to an accelerated phase, or to a rapidly fatal blast crisis within 3–5 years. Blood cells differentiate normally in the stable phase, but not in the blast phase [1,2,4].

Abbreviations: ALL, acute lymphoblastic leukemia; AS, activation segment; CML, chronic myelogenous leukemia; CS or C-spine, catalytic spine; PDGFR, platelet-derived growth factor receptor. Ph^+, Philadelphia chromosome positive, PKA, protein kinase A; pY, phosphotyrosine; RS or R-spine, regulatory spine; Sh1, shell residue-1; SH2, src homology domain-2; STAMP, specifically targeting the Abl myristoyl pocket; VEGFR, vascular endothelial growth factor receptor.

E-mail address: rrj@brimr.org.

https://doi.org/10.1016/j.phrs.2022.106156
Received 2 March 2022; Accepted 2 March 2022
Available online 4 March 2022

The diagnosis of chronic myelogenous leukemia is usually based on detection of the Philadelphia chromosome (Ph) as determined by conventional cytogenetic analysis (karyotyping) and fluorescence in situ hybridization (FISH) analysis of bone marrow samples [1]. Peter Nowell and David Hungerford [5] first described this abnormal chromosome in CML in 1960, and this represents the first specific cytogenetic change associated with a human cancer. Later work showed that the abnormal chromosome was a shortened chromosome 22–the Philadelphia chromosome. Janet Rowley discovered that the Philadelphia chromosome is formed from a reciprocal translocation t(9;22)(q34;q11.2) that results in a lengthened chromosome 9 and a shortened chromosome 22 – the Philadelphia chromosome [6]. The Philadelphia chromosome occurs in about 95% of CML patients and about 25% of patients with ALL (acute lymphoblastic leukemia). It occurs in myelogenous cells (granulocytes), erythroid cells (red cell lineage), megakaryocytes (platelet precursors), monocytes, less commonly in B-lymphocytes, and rarely in T lymphocytes, but not in marrow fibroblasts (non-hematological cells).

The *BCR-ABL* oncogene results from this translocation [7,8]. As a result, the physiological N-terminal inhibitory domain of Abl-1 is eliminated thereby leading to an activated BCR-Abl kinase that stimulates multiple signaling pathways and is the major factor in the pathogenesis of CML. Imatinib was the first drug approved for the treatment of Ph^+ CML, but resistance to imatinib prompted the development of second-generation inhibitors such as bosutinib, dasatinib, and nilotinib, and the third-generation inhibitor called ponatinib [9]. Previous treatments of chronic myelogenous leukemia included hydroxyurea, interferon-α with cytosine arabinoside, and bone marrow transplantation [1]. Although bone marrow transplantation can lead to cures, donors are available for only about 20% of affected people.

In 1980, Owen Witte and co-workers demonstrated [10] that the Abelson leukemia virus oncogene product, v-Abl, is a constitutively active protein-tyrosine kinase. Later work showed that the cellular Abelson leukemia virus homologue gene (c-*ABL*) is moved from chromosome 9 to chromosome 22 where it is combined with the breakpoint cluster region gene (*BCR*) on chromosome 22 [11–14]. BCR-Abl transcripts are measured by quantitative reverse transcriptase polymerase chain reaction (qPCR) methodologies on bone marrow samples (at the time of initial diagnosis) or peripheral blood samples (during treatment). The consequence of the *BCR-ABL* translocation is the creation of a BCR-Abl fusion protein, a constitutively active cytoplasmic protein-tyrosine kinase [15,16]. Owing to the variability of the sites of disruption in the BCR gene, three chimeric gene products have been described: p210 BCR-Abl, p190 BCR-Abl, and p230 BCR-Abl. These proteins contain the same segment of Abl-1 but variable regions of BCR [4]. p210 BCR-Abl is associated with chronic myelogenous leukemia; p190 BCR-Abl and p230 BCR-Abl are associated with other forms of leukemia. Insertion of a retrovirus encoding p210 BCR-Abl into cells of mice promotes the development of a condition closely resembling chronic myelogenous leukemia, giving support to the hypothesis that the *BCR-ABL* hybrid gene is responsible for this disease [16–18].

Chronic myelogenous leukemia, at least in the stable phase, is unique among malignancies in that the malady appears to be the result of a single major biochemical defect [1,16]. In contrast, most malignancies are the result of several genetic and biochemical lesions [19]. Additional mutations account for disease progression from the stable phase to the accelerated and blast phases of CML. The BCR-Abl oncoprotein, an activated protein-tyrosine kinase, thus represents a unique drug target that differs between normal and leukemic cells. Imatinib was approved by the FDA for the treatment of CML in 2001 and the usefulness of this small molecule protein kinase inhibitor in the treatment of cancer played a significant role in the development of additional protein kinase antagonists. There are currently 70 FDA-approved therapeutic protein kinase inhibitors (Supplementary material). Reflecting their importance, perhaps one-quarter to one-third of all current drug discovery efforts worldwide target protein kinases.

2. Biochemistry of Abl

Abl-1a/b is a nonreceptor protein-tyrosine kinase and the human ortholog of the murine Abelson leukemia virus. Abl-1a/b plays a key role in many processes linked to cell growth and survival such as cytoskeleton and actin remodeling, cell motility and adhesion, receptor endocytosis, and autophagy. Abl-1a/b is also translocated into the nucleus where it has DNA-binding activity and is involved in the DNA-damage response and apoptosis. Many of its substrates are mediators of DNA repair including the following gene products: *DDB1* (DNA-damage binding protein-1), *DDB2* (DNA-damage binding protein-2), *ERCC3* (General transcription and DNA repair factor IIH helicase subunit XPB), *ERCC6* (DNA excision repair protein ERCC-6), *RAD9A* (Cell cycle checkpoint control protein RAD9A), *RAD51* (DNA repair protein RAD51 homolog 1), *RAD52* (DNA repair protein RAD52 homolog), and *WRN* (Werner syndrome ATP-dependent helicase) [20,21]. Abl-1a/b activates the proapoptotic pathway when the DNA damage is too severe to be repaired.

Studies by Manning et al. indicated that the human protein kinase family contains 478 typical and 40 atypical enzymes [22]. Protein kinases catalyze the following general reaction:

$$MgATP^{1-} + \text{protein–O:H} \rightarrow \text{protein–O:}PO_3^{2-} + MgADP + H^+$$

Based upon the identity of the protein–OH groups, these enzymes consist of protein-tyrosine kinases (with 90 members), protein-tyrosine kinase–like enzymes (43) and protein-serine/threonine kinases (385). The protein-tyrosine kinase group includes both intracellular nonreceptor (32) proteins such a Abl-1a/b and transmembrane receptors (58). A small group of intracellular protein kinases including MEK1/2 catalyzes the phosphorylation of both tyrosine and then threonine residues within the activation segment of their target protein kinases; MEK1/2 and related enzymes are classified as dual specificity protein kinases. Back-of-the-envelope estimates suggest that about one in every 40 human genes (518 protein kinase genes out of an estimated 20,000 human protein-encoding genes) codes for a protein kinase. Consequently, protein kinases make up about 2.5% of the human genome. Based upon a comprehensive study, Manning et al. reported that 244 protein kinases map to cancer amplicons and other disease loci [22]. This suggests that a significant increase in the number of protein kinase therapeutic targets will be forthcoming as new research into the pathogenesis of currently untargeted diseases is performed.

Alternative splicing of Abl-1 pre-mRNA yields two transcripts: 1a and 1b. The latter is 19 residues longer and it bears a covalently attached myristoyl group that is added post-translationally to a glycine residue immediately following the initiating amino-terminal methionine (Fig. 1) [23]. The myristoyl group plays an essential role in the regulation of Abl-1b while the regulation of Abl-1a remains a mystery. The amino terminus of Abl-1b consists of about 60 residues called the cap. It is followed by the SH3 domain. Such domains (≈60 amino acid residues) bind to sequences that can adopt a left-handed helical conformation [24]. The SH3 domain is a β-barrel consisting of five antiparallel β-strands and a prominent structure called the RT loop (Fig. 2). This loop lies at the ends of a surface composed of hydrophobic and aromatic residues that make up the recognition site for protein sequences that bear the PxxP motif. The side chain N–H group of N97 of the RT loop of Abl-1b forms a hydrogen bond with the carbonyl side chain of N250 of the SH2-kinase linker (not shown). The –OH group of S94 of the RT loop hydrogen bonds with the carbonyl group of K281 within the β2-β3 loop of the small lobe of the kinase domain (SH1).

The SH3-SH2 connector is a six-residue segment that links these two domains together. SH2 domains (≈100 amino acid residues) bind to distinct amino acid sequences C-terminal to phosphotyrosine [25]. The Abl-1a/b SH2 domain (Fig. 2) consists of a central three-stranded β-sheet with a single helix packed against each side (α1 and α2). The SH2 domain forms two recognition pockets: one co-ordinates

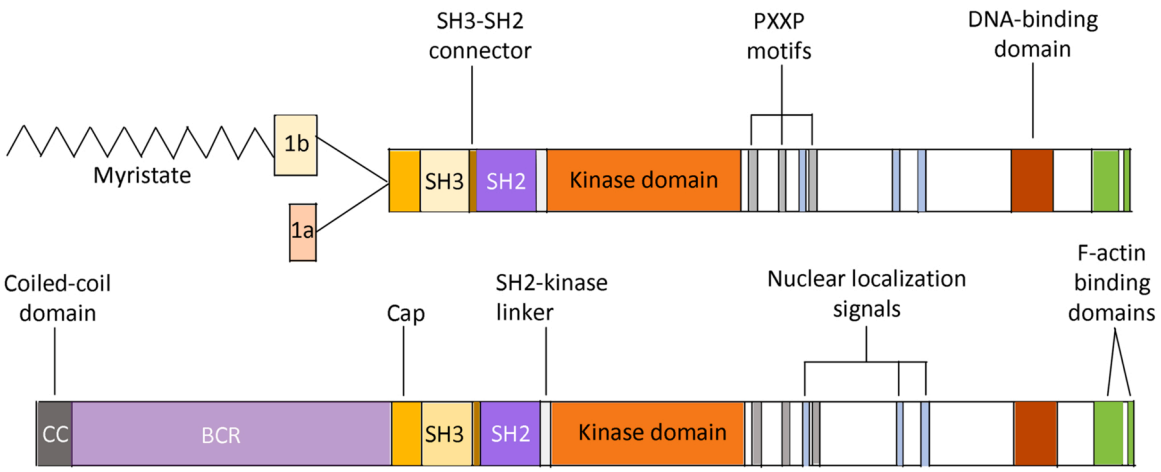

Fig. 1. Diagrammatic representation of the Abl-1a/Abl-1b, and BCR-Abl structures. The figure is not drawn to scale. Adapted from Ref. [29]

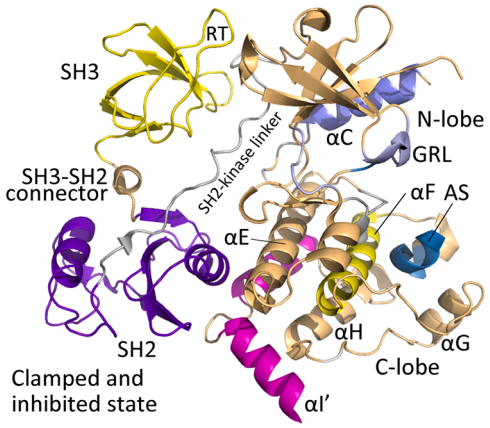

Fig. 2. Overview of the structure of Abl-1b illustrating the SH1-SH2 inhibitory domains including the RT loop interacting with the protein kinase domain (SH1). PDB ID: 5mo4. AS, activation segment.

phosphotyrosine and the other binds one or more hydrophobic residues C-terminal to the phosphotyrosine. The phosphotyrosine pocket contains a conserved arginine residue (Arg171 in human Abl-1b). Songyang and Cantley analyzed the binding of a library of phosphopeptides to SH2 domains to define preferred docking sequences [26]. The SH2 domain of Abl-1a/b selects pYENP in preference to other sequences. However, the Abl-1a/b SH2 domain can bind to a variety of residues that do not conform to this optimal sequence.

The SH3 and SH2 domains interact with the SH1 (protein kinase) domain of Abl-1b. Like all protein kinases, the Abl-1b SH1 domain contains a small N-terminal lobe and large C-terminal lobe [27,28]. The active site is located between the small and large lobes on the side opposite that of the SH3 and SH2 domains. The small and large lobes of the catalytically active Abl-1b must be able to move (breath) in order to affect phosphorylation of its substrates. To maintain the Abl-1b kinase in a quiescent state, the SH3 domain, the SH3-SH2 connector, the SH2 domain, and the SH2-kinase linker dock tightly to the SH1 (protein kinase) domain and function as a clamp to restrict its mobility and inhibit its activity.

Studies at the turn of this century defined the role of the myristoyl group attached to the N-terminus of Abl-1b in the regulation of kinase activity [29]. Hantschel et al. reported that the *ABL1b* glycine-to-alanine mutation at position 2 (*G2A*) led to an enzyme with dramatically higher enzyme activity than wildtype Abl-1b [30]. Conversion of glycine to any other residue renders the protein incapable of being myristoylated in a reaction catalyzed by the N-myristoyltransferase. The first five residues of Abl-1b are MGQQP, which will support N-myristoyltranferase activity, and those of Abl-1a are MLEIC, which will not. Also, in contrast to the wildtype enzyme, the *G2A* mutant protein was highly phosphorylated. These studies suggested that the myristoyl group functions as a negative regulator of Abl-1b phosphotransferase activity. In a collaborative study with Hantschel et al. [30], Nagar et al. determined the X-ray crystal structure of mouse Abl-1b with (i) compound P16 and myristate and (ii) imatinib and myristate [31]. They found that the myristoyl group occupied a deep hydrophobic pocket in the base of the large lobe of the protein kinase domain. The myristate binding pocket is a type IV allosteric inhibitor binding site as noted later.

3. Abl-1b protein kinase structure and mechanism

3.1. Primary, secondary, and tertiary structures

As Knighton et al. initially described for protein kinase A (PKA), kinases including Abl-1b possess a small N-terminal lobe and large C-terminal lobe (Fig. 3) [32]. The small lobe is made up of a five-stranded antiparallel β-sheet (β1–β5) and an αC-helix that occurs in active and inactive orientations [33,34]. The N-terminal lobe contains a glycine-rich loop (GRL), sometimes called the P-loop (for interacting with ATP phosphates), which connects the β1- and β2-strands. The Abl-1b loop is made up of GGGQYG and mimics the canonical protein kinase GxGxΦG sequence where the Φ denotes a hydrophobic residue. Protein kinases including Abl-1b contain an AxK signature within the β3-strand and a conserved glutamate near the middle of the αC-helix. A salt bridge occurs between the side chains of the positively charged β3-strand lysine (K) and the negatively charged αC-glutamate (E) in catalytically active protein kinases and this structure corresponds to the "αC_{in}" conformation (Fig. 3A). The αC_{in} conformation is necessary, but not sufficient, for the expression of full enzyme activity. The absence of this salt bridge occurs in catalytically inactive protein kinases and corresponds to the "αC_{out}" conformation (not shown). The transition of the αC_{out} structure to the αC_{in} conformation is required to produce a catalytically active enzyme.

Hanks and Hunter described 12 subdomains (I–VIa, VIb–XI) that make up the overall core structure of protein kinases [35]. A K/E/D/D (Lys/Glu/Asp/Asp) tetrad plays a crucial role in generating the catalytic activity of all protein kinases. The *K* of the tetrad is the lysine of the β3-strand that forms salt bridges with (i) the α-phosphate and (ii) the β-phosphate of ATP, and (iii) the αC-helix glutamate (*E*) to form the αC_{in} structure. Activation segment residues place the phosphorylatable

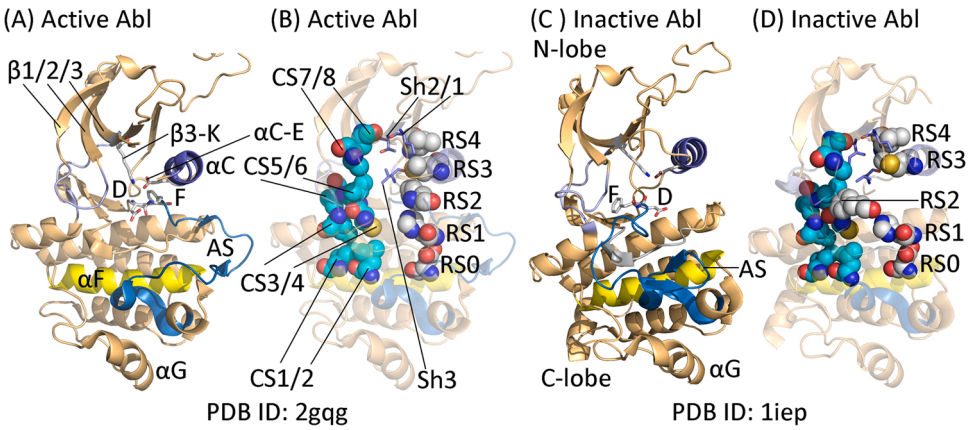

Fig. 3. Structures of active (A & B) and inactive (C & D) Abl. AS, activation segment; CS, catalytic spine; RS, regulatory spine.

substrate into the active site. Moreover, the catalytic-loop HRD-aspartate (the first *D* of the K/E/*D*/D tetrad), functions as a proton acceptor [36]. Additionally, Zhou and Adams hypothesized that the HRD-aspartate positions the –OH group of the protein substrate to facilitate the in-line nucleophilic attack of the oxygen with the γ-phosphate of ATP [37]. See Table 1 for a list of the important Abl-1a/b residues and Ref. [38–40] for a comprehensive summary of protein kinase enzymology.

The second *D* of the K/E/D/*D* tetrad is the first residue of the protein-substrate–binding activation segment. This protein kinase segment begins with DFG and ends with APE or a similar triad such as PPE. Activation segments, which are important structural and regulatory components of all protein kinases, are about 30 residues long [39] (the Abl-1b activation segment contains 29 residues). The catalytic loop of protein kinases is made up of an HRD(x)$_4$N signature. The primary structure of the activation segment occurs after the catalytic loop. Two Mg^{2+} ions – Mg^{2+}(1) and Mg^{2+}(2) – are required for the catalytic activity of almost all protein kinases. The first magnesium ion – Mg^{2+}(1) – interacts with DFG-D of the activation segment and the second magnesium ion – Mg^{2+}(2) – interacts with the terminal asparagine (N) of the catalytic loop [41].

The primary structure and length of the middle region of the activation segment vary greatly among the members of the protein kinase superfamily [27]. The activation segment of Abl-1b, like that of nearly all members of the protein kinase superfamily, contains a residue (Y412, human Abl-1b numbering) that undergoes phosphorylation. Moreover, activation segment phosphorylation is required for the expression of maximal enzyme activity in nearly all protein kinases. The initial part (DFG) of the activation segment is close to the conserved catalytic loop HRD sequence and the beginning of the αC-helix. This helix, which is found within the N-terminal lobe, nevertheless occupies a strategically important position between both lobes. The activation segment of protein kinases has an open and extended structure in the active form of all protein kinases (Fig. 3A) and a closed structure in most quiescent kinases (Fig. 3C) [27]. The two initial residues of the activation segment (DF) occur in different conformations. The DFG-D side chain of active protein kinases points toward the ATP-binding site and it binds Mg^{2+}(1). This arrangement is called the "DFG-D_{in}" conformation (Fig. 3A). In the inactive activation segment configuration that is observed in many protein kinase structures, the DFG-D is directed away from the ATP-binding site. This structure is called the "DFG-D_{out}" conformation (Fig. 3C). It is the ability of DFG-*D* to bind (DFG-D_{in}) or not bind (DFG-D_{out}) Mg^{2+}(1) within the active site that is important.

Modi and Dunbrack performed a comprehensive study of the interaction of drugs with active and inactive conformations of protein kinases based upon the organization of the activation segment, which begins with the DFG sequence [42,43]. This signature sequence is observed in two major classes of conformations: DFG-D_{in} and DFG-D_{out}. In the first instance the phenylalanine residue contacts the αC-helix of the small lobe and in the second instance phenylalanine occupies a portion of the ATP site and produces an αC-helix pocket. These investigators found a grouping of protein conformations that depended upon the position of the phenylalanine side chain (DFG-D_{in}, DFG-D_{out}, and DFG-$D_{intermediate}$) and the backbone dihedral angles of the xDF sequence (where x is the residue before the DFG signature). They identified eight distinctive conformations based on the Ramachandran regions (A, alpha; B, beta; L, left) of the xDF motif and the configuration (χ1) of the phenylalanine rotamer (minus, plus, trans). Their groupings divide the DFG-D_{in} configuration into six clusters including BLAminus, which contains active structures, and two common inactive forms, BLBplus and ABAminus. DFG_{out} structures exist mainly in the BBAminus configuration. The inactive conformations possess features that prevent their binding to ATP, magnesium, and/or their protein substrates. Modi and Dunbrack produced a valuable and noncommercial web site (http://dunbrack3.fccc.edu/kincore/) that enables investigators to determine whether a protein kinase conformation corresponds to an active enzyme (DFG-D_{in}, BLAminus) or to an inactive enzyme (DFG-D_{in}, BLBplus, DFG-D_{in}, ABAminus, DFG-D_{out}, BBAminus). We used this web site to determine whether the conformations of the various drug-enzyme complexes that we are considering are active (DFG-D_{in}, BLAminus) or dormant (otherwise). Table 2 provides a comparison of the BRIMR and the Modi-Dunbrack schemes for describing ligand-kinase interactions. See Refs. [27,42,43] for more information about these and related DFG activation segment arrangements.

Table 1
Important residues in human Abl-1a and Abl-1b protein kinases.

	Abl-1a	Abl-1b
Number of residues	1130	1149
Protein kinase domain	292–493	311–512
Glycine-rich loop	^{249}GGGQYG^{254}	^{268}GGGQYG^{273}
The β3-*K* of *K*/E/D/D	271	290
αC-*E* of K/*E*/D/D	286	305
Hinge-linker residues	^{316}EFMTYGN^{322}	^{335}EFMTYGN^{341}
Gatekeeper residue	T315	T334
Catalytic HR*D* residue, the first *D* of K/E/*D*/D	D344	D363
Catalytic loop	^{361}HRDLAARN^{368}	^{380}HRDLAARN^{387}
AS[a] *D*FG, the second *D* of K/E/D/*D*	D381	D400
AS[a] tyrosine phosphorylation site	Y393	Y412
End of the AS[a]	^{407}APE^{409}	^{426}APE^{428}
Molecular weight (kDa)	122.8	124.9
UniProtKB ID	P00519–1	P00519–2

[a] AS, activation segment.

Table 2
Blue Ridge Institute for Medical Research (BRIMR), Modi-Dunbrack Fox Chase Cancer Center (FCCC), and Kinase Ligand Interaction and Fingerprint and Structure (KLIFS) ligand-inhibitor data base comparisons.

Ligand/ Drug-enzyme	PDB ID	BRIMR type[a]	FCCC type[b,c]	FCCC: Dihedral angles & DFG-D[c]	KLIFS pockets[d]
ADP-AurkA	4dee	I	1	BLAminus & DFG-D_{in}	F, FP-II
BRIMR type I inhibitors					
Dasatinib-Abl	2gqg	I	1.5_back	BLAminus & DFG-D_{in}	F, G, B, BP-I-A/B
BRIMR type IIA inhibitors					
Imatinib-Abl[e]	1iep	IIA	2	BBAminus & DFG-D_{out}	F, G, B, BP-I-A/B, BP-II-out, BP-IV
Nilotinib-Abl	3cs9	IIA	2	BBAminus & DFG-D_{out}	F, G, B, BP-I-A/B, BP-II-out, BP-V
Ponatinib-Abl[e]	3oxz	IIA	2	BBAminus & DFG-D_{out}	F, G, B, BP-I-A/B, BP-II-out, BP-III, BP-IV
BRIMR type IIB inhibitors					
Bosutinib-Abl	3ue4	IIB	1	Unassigned & DFG-D_{out}	F, G, BP-II-A/B

[a] Ref. [28]
[b] b, back
[c] From Refs. [42,43] and http://dunbrack3.fccc.edu/kincore/
[d] klifs.net
[e] Mouse enzyme

3.2. Protein kinase hydrophobic skeletons

Kornev et al. studied the three-dimensional structures of about two dozen active and inactive protein kinases to identify structurally and functionally important residues [44,45]. Their studies revealed an arrangement of four amino acids that make up a regulatory or R-spine and an arrangement of eight amino acids along with the adenine base of ATP that make up a catalytic or C-spine. These residues occur in both the N-terminal and C-terminal lobes. The catalytic and regulatory spines generate a stable, but flexible, catalytically active ensemble. The C-spine helps to position ATP and the R-spine helps to position the protein substrate for catalysis. The regulatory spine contains components from both the activation segment and αC-helix, whose structures are important in determining active and quiescent enzyme states. The precise positioning and alignment of both spines are necessary, but not sufficient, for the formation of a catalytically competent protein kinase.

The R-spine contains the first residue of the β4-strand and the amino acid exactly four residues C-terminal to the conserved αC-helix glutamate, which are within the small lobe [44]. The R-spine also contains the HRD-histidine of the catalytic loop and the activation segment DFG-phenylalanine, both occurring within the large lobe. The HRD-histidine N–H backbone hydrogen bonds with the side chain of a conserved aspartate residue within the hydrophobic αF-helix. From the bottom to the top, Meharena et al. labeled the R-spine residues as RS0, RS1, RS2, RS3, and RS4 [46]. We later labeled the C-spine residues from the bottom to the top as residues CS1–8 [28]. The regulatory and catalytic spines of active protein kinases are linear (Fig. 3B). In protein kinases with the αC_{out} structure, RS3 is displaced rightward as protein kinases are usually depicted (not shown). In protein kinases with the DFG-D_{out} structure, the DFG-D residue (RS2) is displaced toward the left and the R-spine is broken (Fig. 3D). The R-spine, C-spine, and shell residues of Abl-1a/b protein kinases are listed in Table 3.

The protein kinase spine and shell residues play a key role in the structure and activity of these enzymes; it is not possible to overemphasize their importance in the functioning of this enzyme superfamily as well as their interactions with small molecule protein kinase blockers. For a review of the properties of the spine and shell residues

Table 3
Spine and shell residues of human Abl-1a and Abl-1b.

	Symbol	KLIFS No.[a]	Abl-1a	Abl-1b
β4-strand (N-lobe)	RS4	38	L301	L320
C-helix (N-lobe)	RS3	28	M290	M309
Activation loop DFG-F (C-lobe)	RS2	82	F381	F400
Catalytic loop HRD-H (C-lobe)	RS1	68	H361	H380
F-helix (C-lobe)	RS0	None	D421	D440
Two residues upstream from the gatekeeper	Sh3	43	I313	I332
Gatekeeper, end of β5-strand	Sh2	45	T315	T334
αC-β4 loop	Sh1	36	V299	V318
β3-AxK motif (N-lobe)	CS8	15	A269	A288
β2-strand (N-lobe)	CS7	11	V256	V275
β7-strand (C-lobe)	CS6	77	L370	L389
β7-strand (C-lobe)	CS5	78	V371	V390
β7-strand (C-lobe)	CS4	76	C369	C388
D-helix (C-lobe)	CS3	53	L323	L342
F-helix (C-lobe)	CS2	None	L428	L447
F-helix (C-lobe)	CS1	None	I432	I451

[a] From Refs. [82–84].

and their interactions with small molecule inhibitors of selected members of the protein kinase superfamily, see the following papers: Refs. [47,48] for the Src nonreceptor protein-tyrosine kinase, Ref. [49] for the Bruton nonreceptor protein-tyrosine kinase, Ref. [50] for the Janus nonreceptor protein-tyrosine kinase, Refs. [51–53] for the ALK pleotrophin and midkine receptor protein-tyrosine kinase, Refs. [54–56] for the EGFR family of protein-tyrosine kinases, Ref. [57] for the fibroblast growth factor receptor family of protein-tyrosine kinases, Ref. [58] for the Kit stem cell receptor protein-tyrosine kinase, Ref. [59] for the PDGFRα/β protein-tyrosine kinases, Ref. [60] for the RET glial-cell derived receptor protein-tyrosine kinase, Ref. [61] for the VEGFR1/2/3 protein-tyrosine kinases, Ref. [62] for the Flt3 receptor protein-tyrosine kinase, Ref. [63] for the ROS1 orphan receptor protein-tyrosine kinase, Refs. [64,65] for the Raf protein-serine/threonine kinases, Refs. [66,67] for the ERK1/2 protein-serine/threonine kinases, Refs. [68,69] for the cyclin-dependent protein-serine/threonine kinase family, Ref. [70,71] for the MEK1/2 dual specificity protein kinases, and Ref. [72] for phosphatidylinositol 3-kinase, a member of the atypical protein kinase family.

The C-spines of protein kinases consist of two residues from the small lobe and six residues from the large lobe. The adenine base of ATP combines these two parts of the catalytic spine to enable the merging of the two lobes of the enzyme and ready the enzyme for catalysis [45]. The two small lobe residues that bind to the top of the ATP adenine base include the conserved β2-strand valine (CS7) following the glycine-rich loop and the invariant β3-strand alanine (CS8) of the AxK motif. A hydrophobic residue from the middle of the large lobe β7-strand (CS6) interacts with the bottom of the adenine base of ATP. Additionally, CS4 and CS5 interact with CS3 at the beginning of the αD-helix. And CS3 makes hydrophobic contact with the adjacent CS4 as well as CS1 within the αF-helix below it. Both the catalytic and regulatory spines interact with the hydrophobic αF-helix below them; the αF-helix functions as a major foundation for the stabilization of the entire protein kinase domain and it contains CS1, CS2, and RS0 (Fig. 3B/D). The protein kinase hinge and linker residues connect the small and large lobes of protein kinases and the 6-amino group of ATP/ADP hydrogen bonds with the backbone carbonyl group of the first hinge residue. Moreover, the *N*1 of the adenine base of ATP/ADP hydrogen bonds with the backbone N–H group of the third hinge residue (not shown). Nearly all ATP small-molecule steady-state competitive protein kinases inhibitors hydrogen bond with backbone hinge residues, usually with that of the third hinge residue [27].

Based upon the results of site-directed mutagenesis studies, Meharena et al. identified three residues in murine PKA that strengthen the regulatory spine, which they identified as shell residues (Sh1, Sh2, and

Sh3) [46]. While their Sh1 mutant (V104G) possessed 5% of the catalytic activity of the wild type enzyme, their Sh2/Sh3 double mutant (M120G/M118G) was devoid of any activity. These results showed that the shell residues support protein kinase A activity. We infer that shell residues play a similar supporting role for all protein kinases including Abl-1a/b. The Sh1 residue occurs within the segment connecting the αC-helix and the β4-strand, the so-called back loop. The Sh2 residue is the gatekeeper that occurs at the end of the β5-strand immediately before the hinge region and the Sh3 residue is found within the β5-strand two residues upstream from the Sh2 residue (Fig. 3D). Note that *Sh*1/2/3 refers to shell residues while *SH*1/2/3 refers to domains found in members of the protein kinase superfamily.

The term gatekeeper signifies the role that this residue plays in controlling access to the hydrophobic pocket adjoining the adenine binding pocket [73], a pocket that often interacts with structural components of numerous small molecule protein kinase inhibitors. We found that many small molecule therapeutic steady-state ATP-competitive protein kinase antagonists interact with the C-spine (CS6/7/8), the R-spine (RS2/3), and shell (Sh1 and Sh2) residues [74]. Ung et al. reported that about 75% of protein kinases have a relatively large gatekeeper residue (e.g., Met, Leu, Phe) while about 25% have smaller gatekeeper residues (e.g., Thr, Val) [75]. Also of significance in the understanding of long-term drug efficacy, numerous studies indicate that the gatekeeper residue is one of the more common sites of drug-resistant mutations including those of BCR-Abl with the *T315I* resistance mutation (Abl-1a nomenclature) [76,77].

4. Protein kinase-inhibitor classification and inhibitor-binding pockets

Based upon the work of several investigators [78–84], we divided the small molecule protein kinase antagonists into seven main classes that include reversible (Groups I, I½, II, III, IV, and V) and targeted covalent irreversible inhibitors (VI) as defined in Table 4. Asciminib is one of four FDA-approved type IV allosteric protein kinase antagonists. Its allosteric site occurs in the large lobe of the protein kinase domain. In contrast, everolimus, sirolimus, and temsirolimus, classified as type IV inhibitors, promote FKBP12 binding to mTOR, which results in the inhibition of its protein serine-threonine kinase activity. These three macrolides do not directly interact with the protein kinase domain whose activity they block. We divided the type I½ and type II inhibitors into A and B subtypes [28]. Subtype A drugs are those that extend past the gatekeeper residue into the back cleft. In contrast, subtype B drugs are those antagonists that do not extend into the back cleft. The possible significance of this distinction, based on incomplete data, is that subtype A antagonists bind to their protein target with longer residence times than subtype B antagonists [28]. For example, sorafenib is a type IIA VEGFR antagonist and sunitinib is a type IIB VEGFR inhibitor, both of which are FDA-approved for the treatment of renal cell carcinomas. The type IIA drug has a residence time greater than 64 min while the type IIB drug has a residence time less than 2.9 min

Table 4
Classification of small molecule protein kinase inhibitors[a].

Inhibitor type	Properties
I	Binds in and around the ATP-binding pocket of an active enzyme
I½ A/B	Binds in and around the ATP-binding pocket of an inactive DFG-D_{in} enzyme
I½ A	Extends into the back cleft
I½ B	Does not extend into the back cleft
II A/B	Binds in and around the ATP-binding site of an inactive DFG-D_{out} enzyme
II A	Extends into the back cleft
II B	Does not extend into the back cleft
III	Allosteric inhibitor binds near the ATP-binding site
IV	Allosteric inhibitor binds far from the ATP-binding site
V	Bivalent inhibitor spanning two kinase domain regions
VI	Covalent inhibitor

[a] Adapted from Ref. [28].

We followed the lead of several groups in differentiating and defining non type IV allosteric antagonist drug-binding pockets [81–84]. An overview illustrating the location of the pockets and subpockets is provided in Fig. 4. The region between the protein kinase small and large lobes is divided into a front pocket or front cleft, a gate area, and a back cleft. The back pocket (HPII, hydrophobic pocket II) consists of the gate area and the adjoining back cleft. The front cleft includes the glycine-rich loop (GRL), the adenine-binding pocket (AP), the hinge and linker residues that connect the small lobe to the αD-helix in the large lobe, and the catalytic loop $(HRD(x)_4N)$, also in the large lobe.

Type I antagonists typically bind within the front cleft. The gate area includes residues from both lobes. It includes the last three residues of the β3-strand and the first two residues of the β3-αC loop. The gate area also includes the residue immediately before the activation segment (the x of xDFG) along with the first four residues of the activation segment. The back cleft consists of the middle portion of the αC-helix, the β4-strand and the last two residues of the β5-strand. The back cleft also includes the first two and fifth residues of the αE-helix in the large lobe and the two residues preceding the catalytic loop HRD (Fig. 4C). One of the goals in the design and development of small molecule protein kinase antagonists is to maximize selectivity to reduce off-target side effects [79]; this approach can be assisted by assessing drug interactions with target and nontarget enzymes [85–87]. Designing drug fragments that bind to residues lining the various pockets plays a strategic role in protein kinase inhibitor development with the goal of maximizing drug affinity.

van Linden et al. and Kanev et al. described drug and ligand binding to more than 5200 human and mouse protein kinase domains [82,84]. Their KLIFS (kinase–ligand interaction fingerprint and structure) catalog includes an alignment of 85 ligand binding-site residues that are found in both the small and large lobes; their listing aids in the description of drugs and ligands depending upon their binding properties. These data assist in the recognition of common and unique drug-enzyme interactions. These authors formulated a standard amino acid residue numbering system that facilitates the comparison of different protein kinase targets. However, it does not include the interactions of type IV allosteric drugs such as asciminib. Fig. 5 shows the location of the KLIFS residues within the protein kinase domain. Moreover, these authors produced a valuable noncommercial and user-friendly web site that is regularly updated that provides complete data on the interaction of protein kinases with drugs and ligands (klifs.net).

Also of interest, Carles et al. produced a comprehensive list of protein kinase antagonists that have been approved or that are in clinical trials [88]. They created a noncommercial and searchable web site that is regularly updated that includes the structure of the various drugs, their protein kinase targets, therapeutic indications, the year of first approval (if applicable), physical properties, and their trade name (http://www.icoa.fr/pkidb/). Similarly, the Blue Ridge Institute for Medical Research (BRIMR) maintains a web site that lists the FDA-approved protein kinase antagonists and depicts their (i) structures, (ii) molecular weights, (iii) formulas, (iv) number of hydrogen bond donors/acceptors, (v) Log of the partition coefficients and distribution coefficients, (vi) number of rotatable bonds and rings, (vii) year of initial approval, (viii) primary protein kinase targets, (ix) and clinical indications. The site also provides a link to the corresponding FDA labels. This web site (www.brimr.org/PKI/PKIs.htm) is updated following FDA-approval of new protein kinase inhibitors or revisions to the FDA labels.

5. Abl-drug interactions: imatinib, bosutinib, dasatinib, nilotinib, and ponatinib

Imatinib is a 2-amino-4-pyrido-pyrimidine derivative (Fig. 6A) that

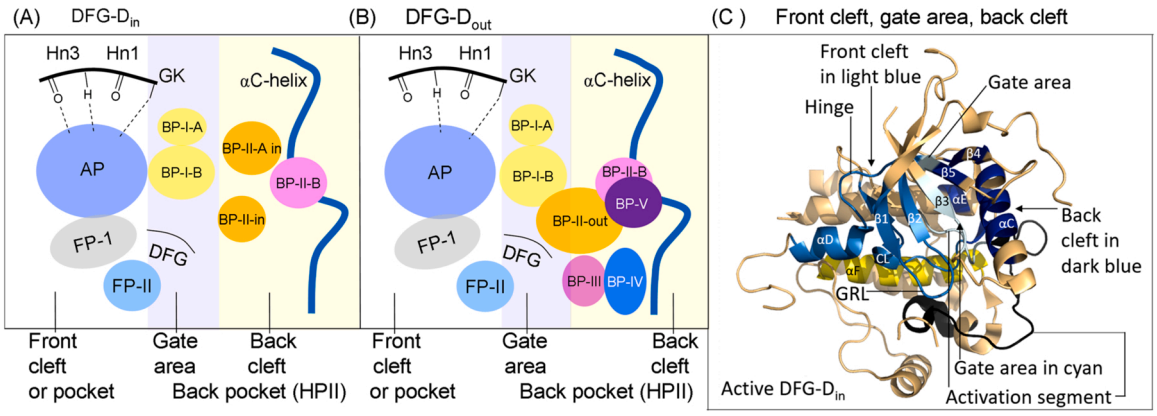

Fig. 4. (A) Location of the protein kinase domain drug-binding pockets in the DFG-D_{in} enzyme form. (B) Location of the drug-binding pockets in the DFG-D_{out} enzyme form. (C) Location of the protein kinase front cleft, gate area, and back cleft. AP, adenine pocket; BP, back pocket; FP, front pocket; Hn, hinge; HPII, hydrophobic pocket II; GK, gatekeeper.
Adapted from Refs. [81–84]

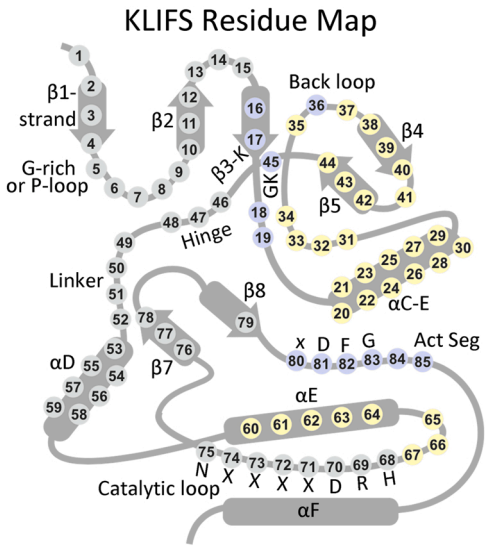

Fig. 5. The location of the KLIFS residues within a generic protein kinase domain. Act Seg, activation segment. Residues in gray circles are in the front cleft; blue, gate area; yellow, back cleft.

is FDA-approved for the treatment of Ph^+ chronic myelogenous leukemia, chronic eosinophilia leukemia, acute lymphoblastic leukemia, hypereosinophilic syndrome, Kit mutation-positive gastrointestinal stromal tumors, dermatofibrosarcoma protuberans, aggressive systemic mastocytosis without the *KIT* ^{D816V} mutation, and myelodysplastic/myeloproliferative diseases with *PDGFR* gene-rearrangements [27,58,64,65–67,89,90]. The drug is a multikinase inhibitor with activity against Abl-1, Abl2, Kit, and PDGFRα/β (klifs.net). The X-ray crystal structure of imatinib bound to Abl-1 shows that the pyridine *N*1 hydrogen bonds with the N–H group of M318 (the third hinge residue) and the amino group hydrogen bonds with the hydroxyl group of the T315 gatekeeper. Additionally, the piperazine *N*4 forms polar bonds with the carbonyl groups of I360 and HRD-H361. The benzamide N–H group hydrogen bonds with the αC-E286 and the benzamide oxygen makes a polar bond with the N–H group of DFG-D381 (Fig. 7A). The drug makes hydrophobic contact with all three shell residues, six spine residues (RS2/3/4 and CS6/7/8), and the KLIFS-3 residue – which occurs immediately before the glycine-rich loop (Table 5). The amino-pyrimidine-pyridine moiety is located in the adenine pocket and the remainder of the drug occupies the gate area (BP-I-A, BP-I-B), BP-II-out, and BP-IV. Based upon the algorithm formulated by Modi and Dunbrack (dunbrack3.fccc.edu/kincore/), Abl-1 has the quiescent DFG-D_{out}-BBAminus structure and they classify it as a type 2 antagonist. The drug binds to inactive Abl with DFG-D_{out} and it extends into the back pocket, which are the properties that we classify as a type IIA inhibitor [28]. The approval of imatinib for the treatment of CML in 2001 paved the way for the discovery and development of all small molecule protein kinase inhibitors [28,77].

Bosutinib is an anilino-quinoline derivative (Fig. 6B) that is a second-generation inhibitor used as a second-line treatment for imatinib-resistant CML not bearing the *T315I* gatekeeper mutation. The drug is a multikinase inhibitor with activity against Abl-1, Src, the Src-family kinases Lck and Yes, and ErbB3 of the epidermal growth factor receptor family (klifs.net). The X-ray crystal structure shows that the *N*1 of the bosutinib quinoline group hydrogen bonds with the N–H group of M318, the third hinge residue (Fig. 7B). The nitrile group of bosutinib extends into gate area hydrophobic pocket BP-I-A near the gatekeeper and its substituted aniline group occupies the gate area hydrophobic pocket BP-I-B. The drug makes hydrophobic contact with five spine residues (RS2/3 and CS6/7/8), all three shell residues, and the KLIFS-3 residue. The drug also makes hydrophobic contact with the β3-strand V270 and K271, M290 of the αC-helix, the β5-strand I313 and I314, ^{317}FMTYG^{321} of the hinge-linker segment, and A380, the x residue immediately before DFG. The Modi-Dunbrack scheme classifies this as a type 1 inhibitor with DFG-D_{out}. In contrast, we classify the interaction as that of a type IIB inhibitor because of the DFG-D_{out} conformation and its localization in the front cleft, gate area, and BP-I-A/B (klifs.net) and its failure to extend past the gate area [28]. The drug is not an effective antagonist of the Abl-1 *T315I* gatekeeper mutant.

Dasatinib is a thiazole-pyrimidine derivative (Fig. 6C) and a second-generation Abl-1 antagonist that is FDA-approved for the second-line treatment of CML not bearing the *T315I* mutation. The drug is a multikinase inhibitor with activity against Abl-1, Abl-2, PDGFRα/β, EphA2/3/5/8, EphB1/2/4/6, and Blk (klifs.net). The X-ray crystal structure shows that the drug forms hydrogen bonds with the T315 gatekeeper residue and M318, the third hinge residue (Fig. 7 C). The drug makes hydrophobic contact with four spine residues (RS3 and CS6/7/8), all three shell residues, and the KLIFS-3 residue. Dasatinib also makes hydrophobic contact with V270 and K271 of the β2-strand, E286 of the αC-helix, ^{317}FMTYG^{321} of the hinge-linker segment, and A380, the x residue immediately before DFG. The Modi-Dunbrack scheme classifies this interaction as type 1.5_back with DFG-D_{in} and BLAminus. The KLIFS scheme has the drug occupying the front cleft, gate area, back cleft, and BP-I-A/B. The BLAminus configuration corresponds to an active enzyme, and we therefore classify this as a type I interaction [28].

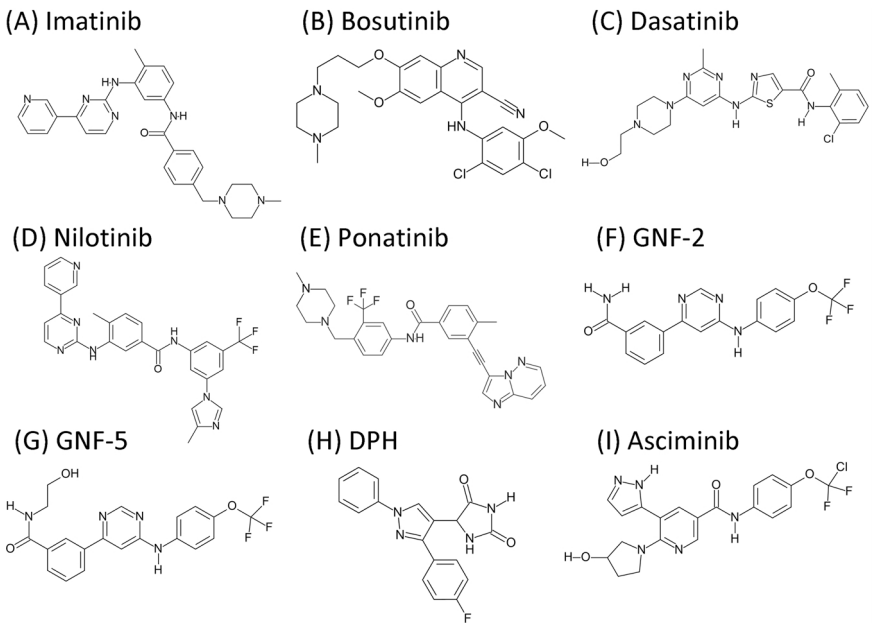

Fig. 6. Structures of Abl ligands.

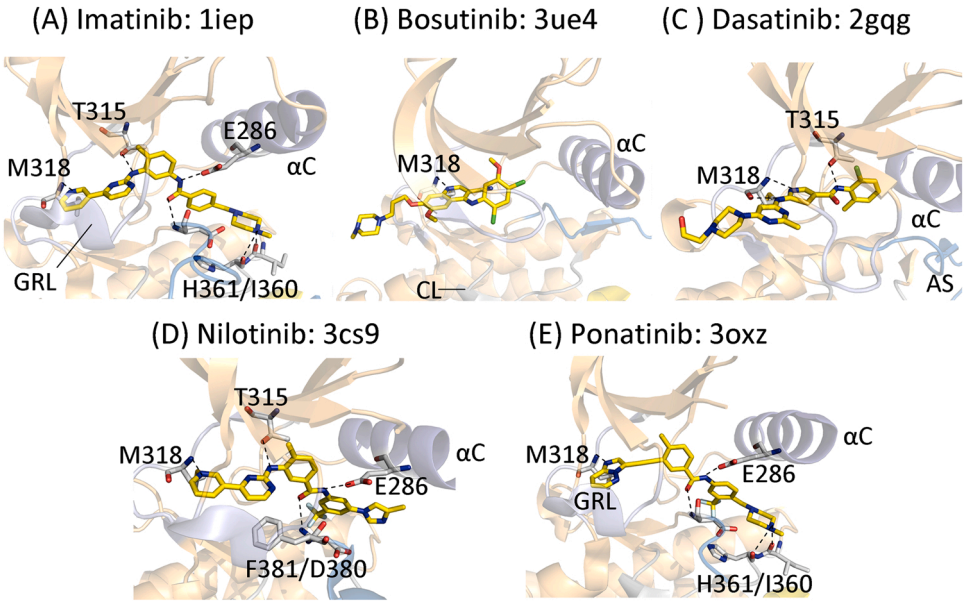

Fig. 7. (A) Abl-imatinib. (B) Abl-bosutinib. (C) Abl-dasatinib. (D) Abl-nilotinib. (E) Abl-ponatinib. The respective PDB ID numbers are listed. The drug carbon atoms are colored yellow and the dashed lines represent polar bonds. AS, activation segment; CL, catalytic loop; GRL, glycine-rich loop.

Nilotinib is a pyridine-pyrimidine derivative (Fig. 6D) that is a second-generation Abl-1 blocker that is FDA-approved for the second-line treatment of CML not bearing the *T315I* mutation. The drug has restricted inhibitory activity and targets only Abl-1 and the epithelial discoidin domain-containing receptor-1 of many enzymes tested (klifs.net). The X-ray crystal structure shows that the drug makes a hydrogen bond with the third hinge residue (M318), the gatekeeper (T315), the αC-helix E286, and DFG-D381. The DFG-D_{out} structure is shown in Fig. 7D. The drug makes hydrophobic contact with six spine residues (RS1/2/3 and CS6/7/8) and with the KLIFS-3 residue. Nilotinib also makes hydrophobic contact with Y253 of the glycine-rich loop, V270 and K271 of the β3-strand, K285, E286, V289, and M290 of the αC-helix, I293 and L298 of the back loop, F317 and M318 of the hinge, G321 of the linker, F359 of the β6-strand, V379 of the β8-strand, A380 (the x of xDFG), and DFG-D381. The drug occupies the front cleft, gate area, back cleft, BP-I-A/B, BP-II-out, BP-III, and BP-V. The Modi-Dunbrack drug-enzyme interaction scheme classifies this as a type 2 complex. Because the drug extends into the back cleft with DFG-D_{out}, we classify nilotinib as a type IIA inhibitor [28].

Ponatinib is an imidazo-pyridine derivative (Fig. 6E) that is a third-generation Abl-1 antagonist that is FDA-approved for the third-line treatment of CML or for the first-line treatment of Abl bearing the *T315I* mutation. The drug is a multikinase antagonist with significant Abl-2, FGFR1/2, PDGFRα/β, Flt3, RET, Src, and Lyn inhibitory activity (klifs.net). The X-ray crystal structure shows that the drug hydrogen bonds with the third hinge residue (M318), αC-E286, I360, HRD-H361, and DFG-D381. Ponatinib makes hydrophobic contact with six spine residues (RS1/2/3 and CS6/7/8), all three shell residues, and the KLIFS-3 residue. It makes hydrophobic contact with Y253 of the glycine-rich loop, V270 and K271 of the β2-strand, E286, V289, M290 of the αC-

Table 5
Drug-Abl hydrophobic (Φ) and hydrogen-bond (A) interactions based upon their common KLIFS residue numbers[a, b, c, d].

	PDB ID	RS1	RS2	RS3	RS4	Sh1	Sh2	Sh3	CS5	CS6	CS7	CS8	KLIFS-3[c]	KLIFS pockets[a]
KLIFS no. →		68	82	28	38	36	45	43	76	77	11	15	3	
Drug-enzyme ↓														
Type I inhibitor														
Dasatinib-Abl	2gqg			Φ		Φ	Φ, A	Φ		Φ	Φ	Φ	Φ	F, G, B, BP-I-A/B
Type IIA inhibitors														
Imatinib-Abl[e]	1iep	Φ, A	Φ	Φ		Φ	Φ, A	Φ		Φ	Φ	Φ	Φ	F, G, B, BP-I-A/B, BP-II-out, BP-IV
Nilotinib-Abl	3cs9	Φ	Φ	Φ		Φ	Φ, A	Φ		Φ	Φ	Φ	Φ	F, G, B, BP-I-A/B, BP-II-out, BP-III, BP-V
Ponatinib-Abl[e]	3oxz	Φ, A	Φ	Φ		Φ	Φ	Φ		Φ	Φ	Φ	Φ	F, G, B, BP-I-A/B, BP-II-out, BP-III, BP-IV
Type IIB inhibitor														
Bosutinib-Abl	3ue4		Φ	Φ		Φ	Φ	Φ		Φ	Φ	Φ	Φ	F, G, BP-II-A/B

[a] klifs.net.
[b] Human enzyme unless otherwise noted.
[c] KLIFS-3, kinase-ligand interaction fingerprint and structure residue-3
[d] A, hydrogen-bond acceptor
[e] Mouse enzyme

helix, I293 and L298 of the back loop, ^{315}TEFM^{318}, G321, and L354 of the αE-helix, F359, I360 of the β6-strand, R362 of the catalytic loop, V379 of the β8-strand, DFG-D381, and A380. The drug occupies the front cleft, gate area, back cleft, BP-I-A/B, BP-II-out, BP-III, and BP-IV. Modi and Dunbrack classify this as a type 2 inhibitor. We classify it as a type IIA inhibitor because it interacts with the DFG-D_{out} configuration and extends past the gate area into the back cleft [28]. As noted later, this drug is associated with several severe toxicities, which limit its usage.

6. Abl-ligand interactions: myristate, GNF-2, DPH, and asciminib

Nagar et al. determined the X-ray crystal structure of mouse Abl-1b with myristate [31]. They found that the myristoyl group occupied a deep hydrophobic pocket in the base of the protein kinase domain containing residues from the αE-helix (A356, L359, L360), the αF-helix (L448, A452, Y454), the αH-helix (C483, P484, V487), and an induced αI'-helix (I521, V525, L529). The terminal nine carbon atoms of myristate occur within the pocket and carbon atoms C2-C5 lie in the broader opening where the side chains of V525 and L529 from the αI'-helix form a shelf for the myristoyl group (Fig. 8A/B). Binding of myristate into its binding pocket induces a bend in the αI-helix to form αI'. Consequently, the SH3-SH2 complex is able to dock tightly with the kinase domain thereby blocking its mobility and catalytic activity. In the absence of the αI-helix bend (Fig. 8E/F), the backside of Abl-1b is unable to dock firmly to the protein kinase domain and the enzyme is active. The myristate binding pocket is a type IV allosteric inhibitor binding site.

Adrian et al. and Zhang et al. performed a phenotypic, differential cytotoxicity screen in an effort to identify new lead compounds that block Abl activity [91,92]. These experiments led to the discovery of GNF-2 (Fig. 6F), which blocked the proliferation of BCR-Abl transformed mouse hematopoietic 32D cells, but it had no effect on the parental cell line. Additional work indicated that GNF-2 blocked the proliferation of murine Ba/F3 cells transformed to be dependent upon wild type and mutant forms of the *BCR-ABL1* gene products that were

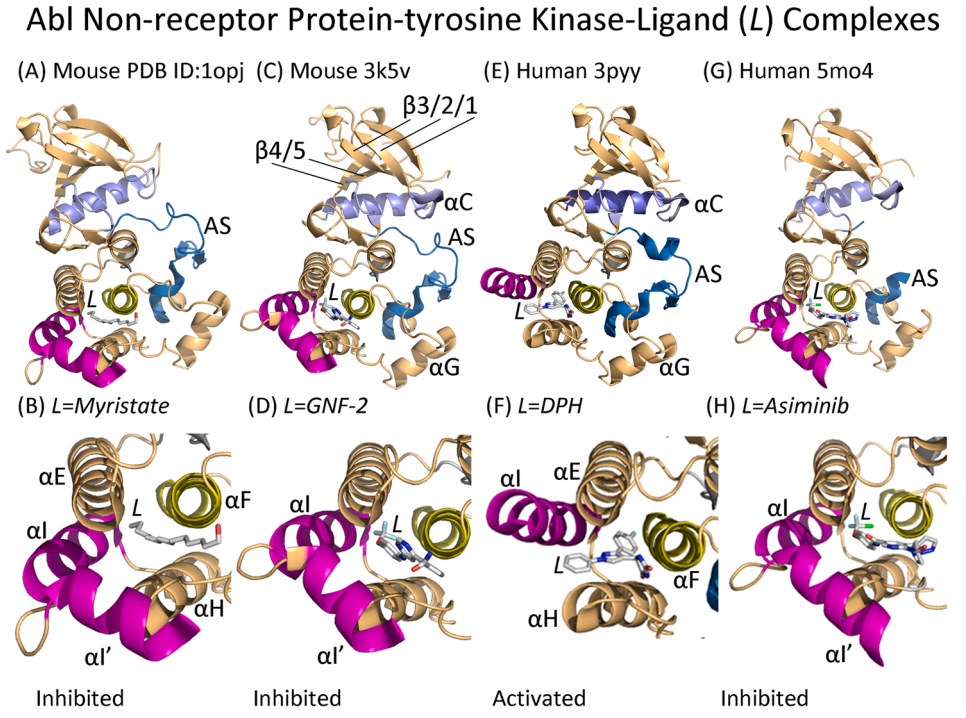

Fig. 8. (A & B) Abl-myristate. (C & D) Abl-GNF-2. (E & F) Abl-DPH. (G & H) Abl-asciminib. The respective PDB ID numbers are listed. The drug carbon atoms are colored gray. AS, activation segment; *L* is the ligand.

resistant to ATP-competitive inhibitors, but the drug was without an effect on the viability of either the parental cell line or cells transfected with other oncogenic protein kinases [93].

Structural studies demonstrated that GNF-2 binds to the myristate-binding site in the large lobe of the protein kinase domain thus mimicking the regulatory role of the myristoyl group of Abl-1b (Fig. 8C/D). GNF-2 makes hydrophobic contact with A356, L359/360, and A363 of the αE-helix, L448, I451, A452, and Y454 of the αF-helix, ^{481}EGCP^{484} and V487 of the αH-helix, F512 and I513 of the αI-helix, and V525 and L529 of the αI'-helix. The GNF-2 allosteric-binding pocket is about 23 Å away from the ATP-binding site and it corresponds to a type IV inhibitor (Table 4) [28]. GNF-2 lacked the appropriate pharmacologic properties to undergo clinical trials, but it served to strengthen the notion that the development of Abl-1b allosteric inhibitors for the treatment of chronic myelogenous leukemia was a feasible option. A related compound, GNF-5 (Fig. 6G), was shown to have activity in a murine leukemic model of CML demonstrating that an allosteric inhibitor bore efficacy in vivo [23]. GNF-2 and GNF-5 are STAMP (specifically targeting the Abl myristoyl pocket) prototypes.

Yang et al. used a high-throughput screening procedure and identified a small molecule cell permeable activator of Abl (5-(1,3-Diaryl-1 H-Pyrazol-4-yl) Hydantoin)) that they named DPH (Fig. 6H) [94]. The X-ray crystal structure showed that it bound to the myristate-binding site of its target. It makes hydrophobic contact with residues of the αE-helix (A356, L359/360, A363), the αF-helix (L448, I451, A452), and the αH-helix (C483, P484 and V487) (Fig. 8E/F). An N–H group from the hydantoin moiety hydrogen bonds with the carbonyl group of E481 (not shown). It does not make contact with the αI-helix and does not induce a bend in the αI-helix thereby explaining its activating effect.

Schoepfer et al. screened about 500 diverse and soluble ligand fragments that bound to Abl-1 using NMR methodology [95]. X-ray crystallography demonstrated that their compounds bound to the myristate-binding site of Abl and they subsequently used general medicinal chemistry approaches to increase drug solubility. These studies were followed by work on lead-derivatives that blocked tumor growth in cell culture and in murine subcutaneous xenograft models of CML. After the development of asciminib (Fig. 6I), they performed a complete characterization of the compound and found that it was very selective as an Abl inhibitor and it had little activity against a battery of other protein kinases. The X-ray crystal structure of asciminib with Abl-1b demonstrates that it makes hydrophobic contact with R351, A356, L359/360, A363 of the αE-helix, L448 and ^{451}IATY^{454} of the αF helix, C483, P484, V487 of the αH-helix, F512 of the αI-helix, and I521, V525, and L529 of the αI'-helix (Fig. 8G/H). The drug also forms a hydrogen bond with E481 (not shown). Of importance, asciminib is active against the *T315I* (Abl-1a nomenclature) gatekeeper mutant. The drug binds to an allosteric site that is not near the ATP-binding site and is now the best example of an FDA-approved type IV antagonist. Asciminib is FDA-approved for the third line treatment of Ph^+ CML and the first line treatment of Ph^+ CML with the *T315I* mutation. See Ref. [96] for a summary of the clinical trials that led to the FDA approval of this STAMP inhibitor.

The data in Table 6 provides a summary and comparison of the residues in the myristate-binding pocket that interact with myristate, GNF-2, DPH, and asciminib. The interaction of these ligands with the αE-, αF-, and αH-helices is quite similar. The three inhibitors interact with the αI-helix, the αI' helix, or both, while the activating DPH does not. Consequently, the αI-helix with bound DPH keeps the SH2/3 complex from docking tightly to the protein kinase domain thereby resulting in increased protein kinase activity. Asciminib has greater affinity for the Abl myristate-binding site than the other ligands and this is correlated with the observation that it makes hydrophobic contact with the binding site residues and it hydrogen bonds with the side chain of E481.

Table 6
Hydrophobic and hydrogen bond (HB) interactions of Abl ligands and myristate pocket residues.

Residue	Myristate	GNF-2	DPH	Asciminib
αE-helix				
R351				+
A356	+	+	+	+
L359	+	+	+	+
L360	+	+	+	+
A363	+	+	+	+
αF-helix				
L448	+	+	+	+
L451		+	+	+
A452	+	+	+	+
T453				+
Y454	+	+		+
αH-helix				
E481		+	HB	HB
G482		+		
C483	+	+	+	+
P484	+	+	+	+
V487	+	+	+	+
αI-helix				
F512		+		+
I513		+		
αI'-helix				
I521	+			+
V525	+	+		+
L529	+	+		+

7. Physicochemical properties of orally effective drugs

7.1. Lipinski's rule of five (Ro5)

Medicinal chemists and pharmacologists have sought the physicochemical properties that result in drugs that are orally effective. Lipinski's rule of five (Ro5) is an experimental and computational methodology that is used to characterize solubility, membrane permeability, and efficacy in the drug-development setting [97]. It is an approximate method that establishes whether an agent with specific pharmacological activities has properties suggesting that it would be orally bioavailable. The Lipinski criteria were grounded on general data showing that most orally effective medicinals are comparatively small and moderately lipophilic molecules. The Ro5 criteria can be used during drug development as pharmacologically active lead compounds are serially optimized to increase their activity while maintaining selectivity and efficacy.

The Ro5 implies that good oral bioavailability is more likely to occur when (i) the atom-based calculated Log P (ALogP) is 5 or less, when (ii) there are 5 or fewer hydrogen-bond donors, when (iii) there are 10 (5 × 2) or fewer hydrogen-bond acceptors, and when (iv) the molecular weight is 500 (5 × 100) or less [97]. The partition coefficient (P) is the ratio of the content of the non-ionized drug in the organic phase of water-saturated *n*-octanol divided by its solubility in the aqueous phase. The P value reflects the hydrophobicity of the ligand or drug; the larger the P value, the greater the hydrophobicity. The number of hydrogen-bond donors is the sum of NH and OH groups. The tally of hydrogen-bond acceptors consists of the number of neutral heteroatoms with the exception of halogen atoms, pyrrole nitrogen atoms, heteroaromatic oxygen and sulfur atoms, and higher oxidation states of sulfur, phosphorous, and nitrogen, but it does include the oxygen atoms bonded to them. The Ro5 is based on the physicochemical characteristics of more than two thousand reference drugs [97]. Asciminib fulfills all of the Ro5 criteria for oral bioavailability (Table 7). Of the other five drugs approved for the treatment of CML, bosutinib, nilotinib, and ponatinib have molecular weights greater than, but close to, 500.

Table 7
Properties of FDA-approved small molecule Abl-1 inhibitors.

Drug	PubMED CID	Formula	MW (Da)	HD[a]	HA[b]	ALogP[c]	Rotatable bonds	PSA[d] (Å^2)	Ring Count[f]	Complexity[e]
Asciminib	72165228	$C_{20}H_{18}ClF_2N_5O_3$	450	3	6	3.46	6	103.4	4	626
Bosutinib	5328940	$C_{26}H_{29}Cl_2N_5O_3$	530	1	8	5.19	9	82.9	4	734
Dasatinib	3062316	$C_{22}H_{26}ClN_7O_2S$	488	3	9	3.31	7	135	4	642
Imatinib	5291	$C_{29}H_{31}N_7O$	494	2	7	4.59	7	86.3	5	706
Nilotinib	644241	$C_{28}H_{22}F_3N_7O$	530	2	9	6.36	6	97.6	5	817
Ponatinib	24826799	$C_{29}H_{27}F_3N_6O$	533	1	8	4.46	6	65.8	5	910

[a] No. of hydrogen bond donors.
[b] No. of hydrogen bond acceptors.
[c] Values for atom-based log of the partition coefficient (ALogP) from https://www.ebi.ac.uk/chembl/.
[d] PSA, polar surface area.
[e] Values obtained from https://pubchem.ncbi.nlm.nih.gov/.
[f] Includes aromatic and nonaromatic rings.

7.2. The importance of lipophilicity and ligand efficiency

7.2.1. Lipophilic efficiency, LipE

After the publication of Lipinski's Ro5 in 2001 [97], subsequent analyses of the physicochemical properties of orally effective medicinals have led to various extensions and refinements [98–105]. Lipophilic efficiency, or LipE, is a feature that is used in drug development and discovery that combines ligand affinity and lipophilic-driven binding as a procedure to increase binding efficacy. The following formulas are used to compute lipophilic efficiency:

$$\text{LipE} = \text{pIC}_{50} - \text{ALogP};\ \text{LipE} = \text{p}K_i - \text{ALogP}$$

Like its usage to express the molar hydrogen ion concentration as pH, the mathematical operator p represents the negative of the Log of the K_i or IC_{50}. Moreover, ALogP is an atom-based computed Log of the partition coefficient; this parameter reflects the ratio of the drug content in the organic phase divided by its solubility in the aqueous phase of immiscible *n*-octanol/water.

The second term of the equation (– ALogP or minus ALogP) denotes the lipophilicity of a drug and the value is computed using an algorithm based upon the physicochemical properties of thousands of reference organic substances. The greater the solubility of a drug in the organic phase of the two-phase *n*-octanol/water mixture, the greater is its lipophilicity, and the more it reduces lipophilic efficiency. Leeson and Springthorpe reported that drug lipophilicity, as assessed by its – ALogP value, is one of the more important properties that should be monitored during drug development [99]. Their use of – ALogP was based upon work performed before the use of the distribution coefficient (D) became more common. The distribution coefficient ($LogD_{7.4}$) represents the ratio of the content of the ionized and non-ionized drug in the organic phase and the aqueous phase of immiscible *n*-octanol/water at a specified pH of the aqueous phase, which is usually 7.4. For practical considerations, either $LogD_{7.4}$ or ALogP can be used to compare a series of compounds during drug development. Hopkins et al. suggested that optimal values of lipophilic efficiency values are greater than ~ 5 and those for LogP are less than ~ 3 [101] and asciminib falls into this category (Table 8). Note that a substance with a large lipophilicity and a large negative (– ALogP) value decreases the lipophilic efficiency.

7.2.2. Ligand efficiency, LE

Ligand efficiency is a procedure for comparing ligand affinities based upon the average binding energy per atom. The ligand efficiency (LE) relates potency, or binding affinity, to the number of heavy (nonhydrogen) atoms of a compound. The following formula is used to calculate this property:

$$\text{LE} = \Delta G^{\circ\prime}/N = -\text{RT}\ \ln K_{eq}/N = -2{\cdot}303\text{RT}\ \text{Log}\ K_{eq}/N$$

$\Delta G^{\circ\prime}$ represents the standard free energy change of a ligand binding to its target enzyme at neutral pH, R is the universal gas constant, (1.98×10^{-3} kcal/degree-mol), T represents the absolute temperature in degrees Kelvin, K_{eq} is the value of the equilibrium constant, and N denotes the number of heavy (nonhydrogen) atoms in the drug. Hopkins et al. reported that optimal values of ligand efficiency should be 0.3 kcal/mol or greater [98,101] and asciminib fulfills this criterion. The K_i or IC_{50} values are proxies for the equilibrium constant. At a physiological temperature of 37 °C (310 K), this equation becomes – ($2.303 \times (1.98 \times 10^{-3}/\text{K}) \times 310$ K Log K_{eq})/N or – 1.41 Log K_{eq}/N. Other authors use a temperature of 300 K and the multiplication factor is – 1.37 [88,92]. Ligand efficiency is especially useful in fragment-based drug discovery protocols and, like lipophilic efficiency, it helps in the selection of derivatives of lead compounds that may be useful for further development [102].

Table 8
Properties of FDA-approved small molecule Abl-1inhibitors [a].

Drug	K_i, nM[a]	pK_i	ALogP[a]	LipE[b]	N[c]	LE[d]	Dosage, mg/day[e]	Solubility, μg/ml[f]	Log $D_{7.4}$[a]	No. aromatic rings	Benzenes	QED[g]
Asciminib	0.5	9.3	3.46	5.84	31	0.3	80–200	54.5	3.86	3	1	0.50
Bosutinib	20	7.7	5.19	2.51	36	0.302	500	9.5	3.37	3	1	0.38
Dasatinib	0.16	9.8	3.31	6.49	33	0.419	100	12.8	3.74	3	1	0.47
Imatinib	1	9	4.59	4.41	37	0.343	600	14.6	3.80	4	2	0.39
Nilotinib	12.5	7.9	6.36	1.54	39	0.286	600 *	2.01	5.35	5	2	0.27
Ponatinib	1	9	4.46	4.54	39	0.325	45	2.95	4.54	4	2	0.39

[a] Representative values obtained from www.ebi.ac.ug/chembl/ and from klifs.net.
[b] LipE = $p\text{IC}_{50}$ – ALogP
[c] N, Number of heavy atoms.
[d] LE = – 2.303 RT Log_{10} K_i/N where N is the number of heavy (non-hydrogen) atoms in the drug.
[e] Dosage from FDA label; *, one-half of total daily dose taken twice per day.
[f] Values from https://go.drugbank.com/drugs/
[g] QED, summed, weighted desirability (scores using MW + ALogP + HBD + HBA + PSA + no. of rotatable bonds + no. of aromatic rings) obtained from https://www.ebi.ac.uk/chembl/; see Ref. [105] for a full explanation.

7.2.3. Additional chemical descriptors of orally effective drugs

To improve drug properties related to oral effectiveness, not-unexpectedly, the Ro5 has generated many corollaries and additions. For example, Veber et al. found that the polar surface area (PSA) and number of rotatable bonds differentiates between orally active and inactive drugs for a large series of substances in rats [103]. They reported that the optimal number of rotatable bonds should be 10 or less. This property is believed to control passive membrane permeation and reflects molecular flexibility (degrees of freedom). Furthermore, the number of degrees of freedom correlates with the entropy change that accompanies ligand binding and determines in part the extent of drug binding to its targets. These authors stated that orally bioavailable medicinals have a polar surface area less than or equal to 140 $Å^2$. All of the drugs approved by the FDA for the treatment of Ph^+ CML, including asciminib, have fewer than ten rotatable bonds and a surface area less than 140 $Å^2$ (Table 7). Moreover, Oprea found that the number of rings (both aromatic and nonaromatic) in most orally approved drugs is three or greater [104]. All of the drugs approved by the FDA for the treatment of CML have this property.

The molecular complexity of an agent is based upon its structural features, symmetry properties, and the elements it contains. The complexity is calculated with the Bertz/Hendrickson/Ihlenfelt algorithm [106,107]. Complexity is based upon the number and identity of the constituent atoms, the nature of the chemical bonds (single, double, triple, aromatic), and the bonding pattern. Molecular complexity ranges from 0 for simple ions to several thousand for complicated natural products. Larger compounds usually possess a higher molecular complexity value than smaller ones. The molecular complexity values for the drugs in this review were acquired from PubChem (https://pubchem.ncbi.nlm.nih.gov/). Of the six drugs that are approved for the treatment of Ph^+ CML, asciminib has the lowest molecular complexity value. There are no optimal or recommended molecular complexity values for orally effective medicines; however, this property may be helpful in determining the ease or difficulty of drug manufacture, an important consideration in the commercial production of pharmaceutical agents.

Ritchie and Macdonald studied the role of aromaticity as it relates to drug efficacy [108]. Aromaticity refers to cyclically conjugated molecules with increased stability owing to electron delocalization. They considered bicyclic and tricyclic structures as containing two and three aromatic rings, respectively. The aromatic ring count includes structures with both carbon and heteroatom components. They report that increasing the number of carboaromatic rings had a detrimental effect on pharmacologic efficacy by decreasing aqueous solubility, increasing binding to serum albumin, and inhibiting CYP450. The ring count of asciminib is four and the number of benzene moieties is one. The values of the other five drugs approved for the treatment of CML were similar with either four or five rings and one or two benzenes (Table 8).

Bayliss et al. evaluated the dose, solubility, and lipophilicity for orally bioavailable drugs and drug candidates [109]. Their work suggested that doses of 100 mg or less daily can reduce the risk of toxicity. The usual dose of asciminib is 80 mg for the treatment of the chronic phase of CML but this is increased to 200 mg in patients with the Abl-1 *T315I* mutation (Table 8). The daily doses of dasatinib and ponatinib are 100 mg daily or less, but those of bosutinib, imatinib, and nilotinib are in the 500–600 mg daily range. Bayliss et al. suggested that drugs with a solubility of less than 100 μg/ml are associated with increased risk of failure during drug development [109]. The solubility of asciminib is greater than that of the other five drugs under consideration, but all of them are less soluble than 100 μg/ml (Table 8).

8. Epilogue

The clinical effectiveness of drugs that are FDA-approved for the treatment of chronic myelogenous leukemia is vastly superior to other protein kinase inhibitors that are used in the treatment of other disorders. Compared with an age-matched normal group, patients with CML have an annual mortality rate from this disorder of 0.5% or less [110,111]. Imatinib (first generation), dasatinib, nilotinib, and bosutinib (second generation) have been FDA-approved for frontline therapy, and ponatinib (third generation) is approved for resistant disease with a *T315I* mutation or after failure with at least two other protein-tyrosine kinase inhibitors [9]. Asciminib is a STAMP inhibitor now approved as a third-line treatment for CML and a first-line treatment in patients with the *T315I* mutation [96]. Pre-clinical studies indicate that using asciminib with an inhibitor targeting the Abl-1 ATP-binding site is effective in preventing the emergence of drug-resistance to either asciminib or the ATP-competitive antagonists. A number of clinical trials using the combination of asciminib with imatinib, bosutinib, or nilotinib are now underway (ClinicalTrials.gov).

The aims of current therapy are to promote patient survival and to achieve treatment-free remission (TFR), whenever possible. For fostering survival, frontline treatment with imatinib, bosutinib, nilotinib, or dasatinib are all effective. If imatinib therapy is used for frontline therapy, a change in therapy at the first evidence of resistant disease is now standard procedure. One reason for using imatinib initially is its availability as a generic drug at a cost lower than that of other agents. The choice of the second line therapy is guided by an evaluation of possible mutations of the Abl kinase domain and by the patient's comorbidities and age [111]. Adverse events produced by bosutinib include diarrhea (10–30%, which is mild and self-limited) and liver and kidney dysfunction. Dasatinib can produce pleural effusions (10–15%), myelosuppression (10–20%), and occasional pulmonary hypertension (1–2%). Nilotinib treatment can produce hyperglycemia (10–15%) and exacerbate diabetes mellitus (5–10%) as well as produce pancreatitis (1–3%). Ponatinib produces the most serious side effects including hypertension (20–30%), vasospastic disease (10–15%), skin rashes (5–10%), and pancreatitis (5%) [111].

Achieving a treatment-free remission is desirable in younger patients to avoid lifetime therapy. A deep molecular response (DMR), which is defined as a 4–4.5 log reduction in the BCR-Abl-1 transcripts on the International Scale (the ratio of BCR-ABL1 transcripts to ABL1 transcripts) or BCR-Abl-1 transcript levels $< 0.01–0.0032\%$, is used as a criterion for discontinuing drug treatment. Discontinuing therapy after a deep molecular response of two-three years is associated with a treatment-free remission rate of 50–60%. When this is done after five years, the probability of achieving a remission rate is greater than 80%. When remission is not achieved, patients respond to the therapy prescribed before drug withdrawal. For additional information on protocols for producing treatment-free remission, see Refs. [2,111]. The concept of treatment-free remission was unthinkable at the beginning of the targeted protein kinase therapy sphere. In the first decade of the 21st century, the idea that drug treatment for CML could be discontinued and the disease would remain abated was a pipedream.

Conflict of interest

The author is unaware of any affiliations, memberships, or financial holdings that might be perceived as affecting the objectivity of this review.

Acknowledgments

I acknowledge the assistance that the late Prof. Janet D. Rowley (1925 – 2013) provided during the early stages of our work on Abl. For a summary of her contributions to science, see Ref. [112]. I thank Dr. Albert J. Kooistra for valuable discussions about the nature of the myristate-binding site and for providing the template depicted in Fig. 5. I express thanks to Laura M. Roskoski for providing editorial and bibliographic assistance. I also thank Jasper Martinsek and Josie Rudnicki for their help in preparing the figures and W.S. Sheppard and Pasha Brezina for their help in structural analyses. The colored figures in this

paper were evaluated to ensure that their perception was accurately conveyed to colorblind readers [113].

Appendix A. Supporting information

Supplementary data associated with this article can be found in the online version at doi:10.1016/j.phrs.2022.106156.

References

[1] M. Baljevic, E. Jabbour, J. Cortes, H.M. Kantarjian, Chronic myeloid leukemia, in: H.M. Kantarjian, R.A. Wolff (Eds.), The MD Anderson Manual of Medical Oncology, third ed., Mc-Graw Hill Education, New York, 2016, pp. 61–80.

[2] J. Cortes, C. Pavlovsky, S. Saußele, Chronic myeloid leukemia, Lancet 398 (2021) 1914–1926, https://doi.org/10.1016/S0140-6736(21)01204-6.

[3] R.L. Siegel, K.D. Miller, H.E. Fuchs, A. Jemal, Cancer statistics, 2022, CA Cancer J. Clin. 72 (2022) 7–33, https://doi.org/10.3322/caac.21708.

[4] R. Kurzrock, H.M. Kantarjian, B.J. Druker, M. Talpaz, Philadelphia chromosome-positive leukemias: from basic mechanisms to molecular therapeutics, Ann. Int. Med. 138 (2003) 819–830, https://doi.org/10.7326/0003-4819-138-10-200305200-00010.

[5] P.C. Nowell, D.A. Hungerford, A minute chromosome in human chronic granulocytic leukemia, Science 132 (1960) 1497.

[6] J.D. Rowley, Letter: A new consistent chromosomal abnormality in chronic myelogenous leukaemia identified by quinacrine fluorescence and Giemsa staining, Nature 243 (1973) 290–293, https://doi.org/10.1038/243290a0.

[7] R. Roskoski Jr., STI-571: an anticancer protein-tyrosine kinase inhibitor, Biochem Biophys. Res. Commun. 309 (2003) 709–717, https://doi.org/10.1016/j.bbrc.2003.08.055.

[8] J. Groffen, J.R. Stephenson, N. Heisterkamp, A. de Klein, C.R. Bartram, G. Grosveld, Philadelphia chromosomal breakpoints are clustered within a limited region, bcr, on chromosome 22, Cell 36 (1984) 93–99, https://doi.org/10.1016/0092-8674(84)90077-1.

[9] E. Jabbour, H. Kantarjian, J. Cortes, Use of second- and third-generation tyrosine kinase inhibitors in the treatment of chronic myeloid leukemia: an evolving treatment paradigm, Clin. Lymphoma Myeloma Leuk. 15 (2015) 323–334, https://doi.org/10.1016/j.clml.2015.03.006.

[10] O.N. Witte, A. Dasgupta, D. Baltimore, Abelson murine leukaemia virus protein is phosphorylated in vitro to form phosphotyrosine, Nature 283 (1980) 826–831, https://doi.org/10.1038/283826a0.

[11] A. de Klein, A.G. van Kessel, G. Grosveld, C.R. Bartram, A. Hagemeijer, D. Bootsma, N.K. Spurr, N. Heisterkamp, J. Groffen, J.R. Stephenson, A cellular oncogene is translocated to the Philadelphia chromosome in chronic myelocytic leukaemia, Nature 300 (1982) 765–767, https://doi.org/10.1038/300765a0.

[12] E. Shtivelman, B. Lifshitz, R.P. Gale, E. Canaani, Fused transcript of *abl* and *bcr* genes in chronic myelogenous leukaemia, Nature 315 (1985) 550–554, https://doi.org/10.1038/315550a0.

[13] Y. Ben-Neriah, G.Q. Daley, A.M. Mes-Masson, O.N. Witte, D. Baltimore, The chronic myelogenous leukemia-specific P210 protein is the product of the *bcr/abl* hybrid gene, Science 233 (1986) 212–214, https://doi.org/10.1126/science.3460176.

[14] N. Heisterkamp, J. Groffen, Philadelphia-positive leukemia: a personal perspective, Oncogene 21 (2002) 8536–8540, https://doi.org/10.1038/sj.onc.1206080.

[15] J.B. Konopka, S.M. Watanabe, O.N. Witte, An alteration of the human c-abl protein in K562 leukemia cells unmasks associated tyrosine kinase activity, Cell 37 (1984) 1035–1042, https://doi.org/10.1016/0092-8674(84)90438-0.

[16] L. Ramakrishnan, N. Rosenberg, *abl* genes, Biochim. Biophys. Acta 989 (1989) 2209–2254, https://doi.org/10.1016/0304-419x(89)90043-7.

[17] G.Q. Daley, R.A. Van Etten, D. Baltimore, Induction of chronic myelogenous leukemia in mice by the $P210^{bcr/abl}$ gene of the Philadelphia chromosome, Science 247 (1990) 824–830, https://doi.org/10.1126/science.2406902.

[18] M.A. Kelliher, J. McLaughlin, O.N. Witte, N. Rosenberg, Induction of a chronic myelogenous leukemia-like syndrome in mice with v-*abl* and *BCR/ABL*, Proc. Natl. Acad. Sci. USA 87 (1990) 6649–6653, https://doi.org/10.1073/pnas.87.17.6649.

[19] D. Hanahan, R.A. Weinberg, Hallmarks of cancer: the next generation, Cell 144 (2011) 646–674, https://doi.org/10.1016/j.cell.2011.02.013.

[20] K. Mahajan, N.P. Mahajan, Cross talk of tyrosine kinases with the DNA damage signaling pathways, Nucleic Acids Res 43 (2015) 10588–10601, https://doi.org/10.1093/nar/gkv1166.

[21] A.A. Bohio, R. Wang, X. Zeng, X. Ba, c-Abl-mediated tyrosine phosphorylation of DNA damage response proteins and implications in important cellular functions (Review), Mol. Med. Rep. 22 (2020) 612–619, https://doi.org/10.3892/mmr.2020.11156.

[22] G. Manning, D.B. Whyte, R. Martinez, T. Hunter, S. Sudarsanam, The protein kinase complement of the human genome, Science 298 (2002) 1912–1934, https://doi.org/10.1126/science.1075762.

[23] P.W. Manley, L. Barys, S.W. Cowan-Jacob, The specificity of asciminib, a potential treatment for chronic myeloid leukemia, as a myristate-pocket binding ABL inhibitor and analysis of its interactions with mutant forms of BCR-ABL1 kinase, Leuk. Res 98 (2020), 106458, https://doi.org/10.1016/j.leukres.2020.106458.

[24] A.A. Adzhubei, M.J. Sternberg, A.A. Makarov, Polyproline-II helix in proteins: structure and function, J. Mol. Biol. 425 (2013) 2100–2132, https://doi.org/10.1016/j.jmb.2013.03.018.

[25] B.A. Liu, B.W. Engelmann, P.D. Nash, The language of SH2 domain interactions defines phosphotyrosine-mediated signal transduction, FEBS Lett. 586 (2012) 2597–2605, https://doi.org/10.1016/j.febslet.2012.04.054.

[26] Z. Songyang, L.C. Cantley, Recognition and specificity in protein tyrosine kinase-mediated signalling, Trends Biochem Sci. 20 (1995) 470–475, https://doi.org/10.1016/s0968-0004(00)89103-3.

[27] R. Roskoski Jr., A historical overview of protein kinases and their targeted small molecule inhibitors, Pharm. Res. 100 (2015) 1–23, https://doi.org/10.1016/j.phrs.2015.07.010.

[28] R. Roskoski Jr., Classification of small molecule protein kinase inhibitors based upon the structures of their drug-enzyme complexes, Pharm. Res 103 (2016) 26–48, https://doi.org/10.1016/j.phrs.2015.10.021.

[29] O. Hantschel, G. Superti-Furga, Regulation of the c-Abl and Bcr-Abl tyrosine kinases, Nat. Rev. Mol. Cell Biol. 5 (2004) 33–44, https://doi.org/10.1038/nrm1280.

[30] O. Hantschel, B. Nagar, S. Guettler, J. Kretzschmar, K. Dorey, J. Kuriyan, G. Superti-Furga, A myristoyl/phosphotyrosine switch regulates c-Abl, Cell 112 (2003) 845–857, https://doi.org/10.1016/s0092-8674(03)00191-0.

[31] B. Nagar, O. Hantschel, M.A. Young, K. Scheffzek, D. Veach, W. Bornmann, B. Clarkson, G. Superti-Furga, J. Kuriyan, Structural basis for the autoinhibition of c-Abl tyrosine kinase, Cell 112 (2003) 859–871, https://doi.org/10.1016/s0092-8674(03)00194-6.

[32] D.R. Knighton, J.H. Zheng, L.F. Ten Eyck, V.A. Ashford, N.H. Xuong, S.S. Taylor, J.M. Sowadski, Crystal structure of the catalytic subunit of cyclic adenosine monophosphate-dependent protein kinase, Science 253 (1991) 407–414, https://doi.org/10.1126/science.1862342.

[33] A.P. Kornev, S.S. Taylor, Dynamics-driven allostery in protein kinases, Trends Biochem Sci. 40 (2015) 628–647, https://doi.org/10.1016/j.tibs.2015.09.002.

[34] S.S. Taylor, J. Wu, J.G.H. Bruystens, J.C. Del Rio, T.W. Lu, A.P. Kornev, L.F. Ten Eyck, From structure to the dynamic regulation of a molecular switch: A journey over 3 decades, J. Biol. Chem. 296 (2021), 100746, https://doi.org/10.1016/j.jbc.2021.100746.

[35] S.K. Hanks, T. Hunter, Protein kinases 6. The eukaryotic protein kinase superfamily: kinase (catalytic) domain structure and classification, FASEB J. 9 (1995) 576–596.

[36] Trafny E.A. Madhusudan, N.H. Xuong, Adams J.A. Ten Eyck, L.F. Taylor, J. M. Sowadski, cAMP-dependent protein kinase: crystallographic insights into substrate recognition and phosphotransfer, Protein Sci. 3 (1994) 176–187, https://doi.org/10.1002/pro.5560030203.

[37] J. Zhou, J.A. Adams, Participation of ADP dissociation in the rate-determining step in cAMP-dependent protein kinase, Biochemistry 36 (1997) 15733–15738, https://doi.org/10.1021/bi971438n.

[38] P.A. Schwartz, B.W. Murray, Protein kinase biochemistry and drug discovery, Bioorg. Chem. 39 (2011) 192–210, https://doi.org/10.1016/j.bioorg.2011.07.004.

[39] A.P. Kornev, S.S. Taylor, Defining the conserved internal architecture of a protein kinase, Biochim Biophys. Acta 1804 (2010) 440–444, https://doi.org/10.1016/j.bbapap.2009.10.017.

[40] R. Lorenz , J. Wu , F.W. Herberg , S.S. Taylor , R.A. Engh , Drugging the undruggable: How isoquinolines and PKA initiated the era of designed protein kinase inhibitor therapeutics. Biochemistry 2021;60:3470–3484. doi: 10.1021/acs.biochem.1c00359.

[41] M.J. Knape, F.W. Herberg, Metal coordination in kinases and pseudokinases, Biochem Soc. Trans. 45 (2017) 653–663, https://doi.org/10.1042/BST20160327.

[42] V. Modi, R.L. Dunbrack Jr., Defining a new nomenclature for the structures of active and inactive kinases, Proc. Natl. Acad. Sci. USA 116 (2019) 6818–6827, https://doi.org/10.1073/pnas.1814279116.

[43] V. Modi, R.L. Dunbrack, Kincore: a web resource for structural classification of protein kinases and their inhibitors, Nucleic Acids Res. (2021), https://doi.org/10.1093/nar/gkab920.

[44] A.P. Kornev, N.M. Haste, S.S. Taylor, L.F. Eyck, Surface comparison of active and inactive protein kinases identifies a conserved activation mechanism, Proc. Natl. Acad. Sci. USA 103 (2006) 17783–17788, https://doi.org/10.1073/pnas.0607656103.

[45] A.P. Kornev, S.S. Taylor, L.F. Ten Eyck, A helix scaffold for the assembly of active protein kinases, Proc. Natl. Acad. Sci. USA 105 (2008) 14377–14382, https://doi.org/10.1073/pnas.0807988105.

[46] H.S. Meharena, P. Chang, M.M. Keshwani, K. Oruganty, A.K. Nene, N. Kannan, S. S. Taylor, A.P. Kornev, Deciphering the structural basis of eukaryotic protein kinase regulation, PLoS Biol. 11 (2013), e1001690, https://doi.org/10.1371/journal.pbio.1001680.

[47] R. Roskoski Jr., Src protein-tyrosine kinase structure, mechanism, and small molecule inhibitors, Pharm. Res 94 (2015) 9–25, https://doi.org/10.1016/j.phrs.2015.01.003.

[48] M.C. Frame, R. Roskoski Jr., Src family tyrosine kinases. Reference Module in Life Sciences, Elsevier,, Amsterdam, 2017, pp. 1–11, https://doi.org/10.1016/B978-0-12-809633-8.07199-5.

[49] R. Roskoski Jr., Ibrutinib inhibition of Bruton protein-tyrosine kinase (BTK) in the treatment of B cell neoplasms, Pharm. Res 113 (2016) 395–408, https://doi.org/10.1016/j.phrs.2016.09.011.

[50] R. Roskoski Jr., Janus kinase (JAK) inhibitors in the treatment of inflammatory and neoplastic diseases, Pharm. Res. 111 (2016) 784–803, https://doi.org/10.1016/j.phrs.2016.07.038.

[51] R. Roskoski Jr., Anaplastic lymphoma kinase (ALK): structure, oncogenic activation, and pharmacological inhibition, Pharm. Res. 68 (2013) 68–94, https://doi.org/10.1016/j.phrs.2012.11.007.
[52] R. Roskoski Jr., Anaplastic lymphoma kinase (ALK) inhibitors in the treatment of ALK-driven lung cancers, Pharm. Res. 117 (2017) 343–356, https://doi.org/10.1016/j.phrs.2017.01.007.
[53] R. Roskoski Jr., The preclinical profile of crizotinib in the treatment of non-small cell lung cancer and other neoplastic disorders, Expert Opin. Drug Dis. 8 (2013) 1165–1179, https://doi.org/10.1517/17460441.2013.813015.
[54] R. Roskoski Jr., The ErbB/HER family of protein-tyrosine kinases and cancer, Pharm. Res. 79 (2014) 34–74, https://doi.org/10.1016/j.phrs.2013.11.002.
[55] R. Roskoski Jr., ErbB/HER protein-tyrosine kinases: Structure and small molecule inhibitors, Pharm. Res. 87 (2014) 42–59, https://doi.org/10.1016/j.phrs.2014.06.001.
[56] R. Roskoski Jr., Small molecule inhibitors targeting the EGFR/ErbB family of protein-tyrosine kinases in human cancers, Pharm. Res. 139 (2019) 395–411, https://doi.org/10.1016/j.phrs.2018.11.014.
[57] R. Roskoski Jr., The role of fibroblast growth factor receptor (FGFR) protein-tyrosine kinase inhibitors in the treatment of cancers including those of the urinary bladder, Pharm. Res. 151 (2020), 104567, https://doi.org/10.1016/j.phrs.2019.104567.
[58] R. Roskoski Jr., The role of small molecule Kit protein-tyrosine kinase inhibitors in the treatment of neoplastic disorders, Pharm. Res. 133 (2018) 35–52, https://doi.org/10.1016/j.phrs.2018.04.020.
[59] R. Roskoski Jr., The role of small molecule platelet-derived growth factor receptor (PDGFR) inhibitors in the treatment of neoplastic disorders, Pharm. Res. 129 (2018) 65–83, https://doi.org/10.1016/j.phrs.2018.01.021.
[60] R. Roskoski Jr., A. Sadeghi-Nejad, Role of RET protein-tyrosine kinase inhibitors in the treatment RET-driven thyroid and lung cancers, Pharm. Res. 128 (2018) 1–17, https://doi.org/10.1016/j.phrs.2017.12.021.
[61] R. Roskoski Jr., Vascular endothelial growth factor (VEGF) and VEGF receptor inhibitors in the treatment of renal cell carcinomas, Pharm. Res. 120 (2017) 116–132, https://doi.org/10.1016/j.phrs.2017.03.010.
[62] R. Roskoski Jr., The role of small molecule Flt3 receptor protein-tyrosine kinase inhibitors in the treatment of Flt3-positive acute myelogenous leukemias, Pharm. Res. 155 (2020), 104725, https://doi.org/10.1016/j.phrs.2020.104725.
[63] R. Roskoski Jr., ROS1 protein-tyrosine kinase inhibitors in the treatment of ROS1 fusion protein-driven non-small cell lung cancers, Pharm. Res. 121 (2017) 202–212, https://doi.org/10.1016/j.phrs.2017.04.022.
[64] R. Roskoski Jr., Targeting oncogenic Raf protein-serine/threonine kinases in human cancers, Pharm. Res. 135 (2018) 239–258, https://doi.org/10.1016/j.phrs.2018.08.013.
[65] R. Roskoski Jr., RAF protein-serine/threonine kinases: structure and regulation, Biochem Biophys. Res. Commun. 399 (2010) 313–317, https://doi.org/10.1016/j.bbrc.2010.07.092.
[66] R. Roskoski Jr., ERK1/2 MAP kinases: structure, function, and regulation, Pharm. Res. 66 (2012) 105–143, https://doi.org/10.1016/j.phrs.2012.04.005.
[67] R. Roskoski Jr., Targeting ERK1/2 protein-serine/threonine kinases in human cancers, Pharm. Res. 142 (2019) 151–168, https://doi.org/10.1016/j.phrs.2019.01.039.
[68] R. Roskoski Jr., Cyclin-dependent protein kinase inhibitors including palbociclib as anticancer drugs, Pharm. Res. 107 (2016) 249–275, https://doi.org/10.1016/j.phrs.2016.03.012.
[69] R. Roskoski Jr., Cyclin-dependent protein serine/threonine kinase inhibitors as anticancer drugs, Pharm. Res. 139 (2019) 471–488, https://doi.org/10.1016/j.phrs.2018.11.035.
[70] R. Roskoski Jr., MEK1/2 dual-specificity protein kinases: structure and regulation, Biochem Biophys. Res. Commun. 417 (2012) 5–10, https://doi.org/10.1016/j.bbrc.2011.11.145.
[71] R. Roskoski Jr., Allosteric MEK1/2 inhibitors including cobimetanib and trametinib in the treatment of cutaneous melanomas, Pharm. Res. 117 (2017) 20–31, https://doi.org/10.1016/j.phrs.2016.12.009.
[72] R. Roskoski Jr., Properties of FDA-approved small molecule phosphatidylinositol 3-kinase inhibitors prescribed for the treatment of malignancies, Pharm. Res. 168 (2021), 105579, https://doi.org/10.1016/j.phrs.2021.105579.
[73] Y. Liu, K. Shah, F. Yang, L. Witucki, K.M. Shokat, A molecular gate which controls unnatural ATP analogue recognition by the tyrosine kinase v-Src, Bioorg. Med. Chem. 6 (1998) 1219–1226, https://doi.org/10.1016/s0968-0896(98)00099-6.
[74] R. Roskoski Jr., Hydrophobic and polar interactions of FDA-approved small molecule protein kinase inhibitors with their target enzymes, Pharm. Res. 169 (2021), 105660, https://doi.org/10.1016/j.phrs.2021.105660.
[75] P.M. Ung, R. Rahman, A. Schlessinger, Redefining the protein kinase conformational space with machine learning, Cell Chem. Biol. 25 (2018), https://doi.org/10.1016/j.chembiol.2018.05.002.
[76] R. Hu, H. Xu, P. Jia, Z. Zhao, KinaseMD: kinase mutations and drug response database, Nucleic Acids Res. 49 (D1) (2021) D552–D561, https://doi.org/10.1093/nar/gkaa945.
[77] P. Cohen, D. Cross, P.A. Jänne, Kinase drug discovery 20 years after imatinib: progress and future directions, Nat. Rev. Drug Disco 20 (2021) 551–569, https://doi.org/10.1038/s41573-021-00195-4.
[78] F. Zuccotto, E. Ardini, E. Casale, M. Angiolini, Through the "gatekeeper door": exploiting the active kinase conformation, J. Med. Chem. 53 (2010) 2691–2694, https://doi.org/10.1021/jm901443h.
[79] L.K. Gavrin, E. Saiah, Approaches to discover non-ATP site inhibitors, Med Chem. Commun. 4 (2013) 41, https://doi.org/10.1039/c2md20180a.
[80] V. Lamba, I. Ghosh, New directions in targeting protein kinases: focusing upon true allosteric and bivalent inhibitors, Curr. Pharm. Des. 18 (2012) 2936–2945, https://doi.org/10.2174/138161212800672813.
[81] J.J. Liao, Molecular recognition of protein kinase binding pockets for design of potent and selective kinase inhibitors, J. Med. Chem. 50 (2007) 409–424, https://doi.org/10.1021/jm0608107.
[82] O.P. van Linden, A.J. Kooistra, R. Leurs, I.J. de Esch, C. de Graaf, KLIFS: a knowledge-based structural database to navigate kinase-ligand interaction space, J. Med. Chem. 57 (2014) 249–277, https://doi.org/10.1021/jm400378w.
[83] A.J. Kooistra, G.K. Kanev, O.P. van Linden, R. Leurs, I.J. de Esch, C. de Graaf, KLIFS: a structural kinase-ligand interaction database, Nucleic Acids Res. 44 (D1) (2016) D365–D371, https://doi.org/10.1093/nar/gkv1082.
[84] G.K. Kanev, C. de Graaf, B.A. Westerman, I.J.P. de Esch, A.J. Kooistra, KLIFS: an overhaul after the first 5 years of supporting kinase research, Nucleic Acids Res. (2020), https://doi.org/10.1093/nar/gkaa895.
[85] B. Wienen-Schmidt, D. Schmidt, H.D. Gerber, A. Heine, H. Gohlke, G. Klebe, Surprising non-additivity of methyl groups in drug-kinase interaction, ACS Chem. Biol. 14 (2019) 2585–2594, https://doi.org/10.1021/acschembio.9b00476.
[86] D. Bajusz, G.G. Ferenczy, G.M. Keserű, Structure-based virtual screening approaches in kinase-directed drug discovery, Curr. Top. Med. Chem. 17 (2017) 2235–2259, https://doi.org/10.2174/1568026617666170224121313.
[87] P. Wu, T.E. Nielsen, M.H. Clausen, FDA-approved small-molecule kinase inhibitors, Trends Pharm. Sci. 36 (2015) 422–439, https://doi.org/10.1016/j.tips.2015.04.005.
[88] F. Carles, S. Bourg, C. Meyer, P. Bonnet, PKIDB: a curated, annotated and updated database of protein kinase inhibitors in clinical trials, Molecules (2018) 23, https://doi.org/10.3390/molecules23040908.
[89] P.M. Fischer, Approved and experimental small-molecule oncology kinase inhibitor drugs: a mid-2016 overview, Med. Res. Rev. 37 (2017) 314–367, https://doi.org/10.1002/med.21409.
[90] F. Rossari, F. Minutolo, Orciuolo E. Past, present, and future of Bcr-Abl inhibitors: from chemical development to clinical efficacy, J. Hematol. Oncol. 11 (2018) 84, https://doi.org/10.1186/s13045-018-0624-2.
[91] F.J. Adrián, Q. Ding, T. Sim, A. Velentza, C. Sloan, Y. Liu, G. Zhang, W. Hur, S. Ding, P. Manley, J. Mestan, D. Fabbro, N.S. Gray, Allosteric inhibitors of Bcr-abl-dependent cell proliferation, Nat. Chem. Biol. 2 (2006) 95–102, https://doi.org/10.1038/nchembio760.
[92] J. Zhang, F.J. Adrián, W. Jahnke, S.W. Cowan-Jacob, A.G. Li, R.E. Iacob, T. Sim, J. Powers, C. Dierks, F. Sun, G.R. Guo, Q. Ding, B. Okram, Y. Choi, A. Wojciechowski, X. Deng, G. Liu, G. Fendrich, A. Strauss, N. Vajpai, S. Grzesiek, T. Tuntland, Y. Liu, B. Bursulaya, M. Azam, P.W. Manley, J.R. Engen, G.Q. Daley, M. Warmuth, N.S. Gray, Targeting Bcr-Abl by combining allosteric with ATP-binding-site inhibitors, Nature 463 (2010) 501–506, https://doi.org/10.1038/nature08675.
[93] M. Warmuth, S. Kim, X.J. Gu, G. Xia, F. Adrián, Ba/F3 cells and their use in kinase drug discovery, Curr. Opin. Oncol. 19 (2007) 55–60, https://doi.org/10.1097/CCO.0b013e328011a25f.
[94] J. Yang, N. Campobasso, M.P. Biju, K. Fisher, X.Q. Pan, J. Cottom, S. Galbraith, T. Ho, H. Zhang, X. Hong, P. Ward, G. Hofmann, B. Siegfried, F. Zappacosta, Y. Washio, P. Cao, J. Qu, S. Bertrand, D.Y. Wang, M.S. Head, H. Li, S. Moores, Z. Lai, K. Johanson, G. Burton, C. Erickson-Miller, G. Simpson, P. Tummino, R. A. Copeland, A. Oliff, Discovery and characterization of a cell-permeable, small-molecule c-Abl kinase activator that binds to the myristoyl binding site, Chem. Biol. 18 (2011) 177–186, https://doi.org/10.1016/j.chembiol.2010.12.013.
[95] J. Schoepfer, W. Jahnke, G. Berellini, S. Buonamici, S. Cotesta, S.W. Cowan-Jacob, S. Dodd, P. Drueckes, D. Fabbro, T. Gabriel, J.M. Groell, R.M. Grotzfeld, A. Q. Hassan, C. Henry, V. Iyer, D. Jones, F. Lombardo, A. Loo, P.W. Manley, X. Pellé, G. Rummel, B. Salem, M. Warmuth, A.A. Wylie, T. Zoller, A.L. Marzinzik, P. Furet, Discovery of asciminib (ABL001), an allosteric inhibitor of the tyrosine kinase activity of BCR-ABL1, J. Med Chem. 61 (2018) 8120–8135, https://doi.org/10.1021/acs.jmedchem.8b01040.
[96] E.D. Deeks, Asciminib: first approval, Drugs 82 (2022) 219–226, https://doi.org/10.1007/s40265-021-01662-3.
[97] C.A. Lipinski, F. Lombardo, B.W. Dominy, P.J. Feeney, Experimental and computational approaches to estimate solubility and permeability in drug discovery and development settings, Adv. Drug Deliv. Rev. 46 (2001) 3–26, https://doi.org/10.1016/s0169-409x(00)00129-0.
[98] A.L. Hopkins, C.R. Groom, A. Alex, Ligand efficiency: a useful metric for lead selection, Drug Disco Today 9 (2004) 430–431, https://doi.org/10.1016/S1359-6446(04)03069-7.
[99] P.D. Leeson, B. Springthorpe, The influence of drug-like concepts on decision-making in medicinal chemistry, Nat. Rev. Drug Disco 6 (2007) 881–890, https://doi.org/10.1038/nrd2445.
[100] S. Ekins, N.K. Litterman, C.A. Lipinski, B.A. Bunin, Thermodynamic proxies to compensate for biases in drug discovery methods, Pharm. Res. 33 (2016) 194–205, https://doi.org/10.1007/s11095-015-1779-y.
[101] A.L. Hopkins, G.M. Keserü, P.D. Leeson, D.C. Rees, C.H. Reynolds, The role of ligand efficiency metrics in drug discovery, Nat. Rev. Drug Disco 13 (2014) 105–121, https://doi.org/10.1038/nrd4163.
[102] P.D. Leeson, Molecular inflation, attrition, and the rule of five, Adv. Drug Deliv. Rev. 101 (2016) 22–33, https://doi.org/10.1016/j.addr.2016.01.018.
[103] D.F. Veber, S.R. Johnson, H.Y. Cheng, B.R. Smith, K.W. Ward, K.D. Kopple, Molecular properties that influence the oral bioavailability of drug candidates, J. Med. Chem. 45 (2002) 2615–2623, https://doi.org/10.1021/jm020017n.
[104] T.I. Oprea, Property distribution of drug-related chemical databases, J. Comput. Aided Mol. Des. 14 (2000) 251–264, https://doi.org/10.1023/a:1008130001697.

[105] P.D. Leeson, A.P. Bento, A. Gaulton, A. Hersey, E.J. Manners, C.J. Radoux, A. R. Leach, Target-based evaluation of "drug-like" properties and ligand efficiencies, J. Med. Chem. 64 (2021) 7210–7230, https://doi.org/10.1021/acs.jmedchem.1c00416.

[106] S.H. Bertz, The first general index of molecular complexity, J. Am. Chem. Soc. 1103 (1981) 3559–3601, https://doi.org/10.1021/ja00402a071.

[107] J.B. Hendrickson, P. Huang, A.G. Toczko, Molecular complexity: a simplified formula adapted to individual atoms, J. Chem. Inf. Compout Sci. 27 (1987) 63–67, https://doi.org/10.1021/ci00054a004.

[108] T.J. Ritchie, S.J. Macdonald, Physicochemical descriptors of aromatic character and their use in drug discovery, J. Med. Chem. 57 (2014) 7206–7215, https://doi.org/10.1021/jm500515d.

[109] M.K. Bayliss, J. Butler, P.L. Feldman, D.V. Green, P.D. Leeson, M.R. Palovich, A. J. Taylor, Quality guidelines for oral drug candidates: dose, solubility and lipophilicity, Drug Disco Today 21 (2016) 1719–1727, https://doi.org/10.1016/j.drudis.2016.07.007.

[110] K. Sasaki, S.S. Strom, S. O'Brien, E. Jabbour, F. Ravandi, M. Konopleva, G. Borthakur, N. Pemmaraju, N. Daver, P. Jain, S. Pierce, H. Kantarjian, J. E. Cortes, Relative survival in patients with chronic-phase chronic myeloid leukaemia in the tyrosine-kinase inhibitor era: analysis of patient data from six prospective clinical trials, Lancet Haematol. 2 (2015) e186–e193, https://doi.org/10.1016/S2352-3026(15)00048-4.

[111] H.M. Kantarjian, N. Jain, G. Garcia-Manero, M.A. Welch, F. Ravandi, W. G. Wierda, E.J. Jabbour, The cure of leukemia through the optimist's prism, Cancer 128 (2022) 240–259, https://doi.org/10.1002/cncr.33933.

[112] Druker BJ. Janet Rowley (1925–2013). Nature 2014;505:484. doi: 10.1038/505484a.

[113] R. Roskoski Jr., Guidelines for preparing color figures for everyone including the colorblind, Pharm. Res. 119 (2017) 240–241, https://doi.org/10.1016/j.phrs.2017.02.005. Erratum in: Pharmacol Res 2019;139:569. doi: 10.1016/j.phrs.2018.09.019.